Fast IPSPs elicited via multiple synaptic release sites by different types of GABAergic neurone in the cat visual cortex

G. Tamás*†, E. H. Buhl* and P. Somogyi*

*MRC Anatomical Neuropharmacology Unit, Department of Pharmacology, University of Oxford, Mansfield Road, Oxford OX1 3TH, UK and
† Department of Zoology and Cell Biology, József Attila University, Szeged, Hungary

1. The effects of synapses established by smooth dendritic neurones on pyramidal and spiny stellate cells were studied in areas 17 and 18 of the cat visual cortex *in vitro*. Paired intracellular recordings with biocytin-filled electrodes and subsequent light and electron microscopic analysis were used to determine the sites of synaptic interaction.

2. All smooth dendritic cells established type II synapses previously shown to be made by terminals containing GABA, therefore the studied cells are probably GABAergic. Three classes of presynaptic cell could be defined, based on their efferent synaptic target preference determined from random samples of unlabelled postsynaptic cells. (a) Basket cells ($n = 6$) innervated mainly somata (49·9 ± 13·8%) and dendritic shafts (45·2 ± 10·7%) and, to a lesser extent, dendritic spines (4·9 ± 4·6%). (b) Dendrite-targeting cells ($n = 5$) established synapses predominantly on dendritic shafts (84·3 ± 9·4%) and less frequently on dendritic spines (11·2 ± 6·7%) or somata (4·5 ± 4·7%). (c) Double bouquet cells ($n = 4$) preferred dendritic spines (69·2 ± 4·2%) to dendritic shafts (30·8 ± 4·2%) as postsynaptic targets and avoided somata.

3. Interneurones formed 5240 ± 1600 (range, 2830–9690) synaptic junctions in the slices. Based on the density of synapses made by single interneurones and the volume density of GABAergic synapses, it was calculated that an average interneurone provides 0·66 ± 0·20% of the GABAergic synapses in its axonal field.

4. The location of synaptic junctions on individual, identified postsynaptic cells reflected the overall postsynaptic target distribution of the same GABAergic neurone. The number of synaptic junctions between pairs of neurones could not be predicted from light microscopic examination. The number of electron microscopically verified synaptic sites was generally smaller for the dendritic domain and larger for the somatic domain than expected from light microscopy. All presynaptic cells established multiple synaptic junctions on their postsynaptic target cells. A basket cell innervated a pyramidal cell via fifteen release sites; the numbers of synapses formed by three dendrite-targeting cells on pyramidal cells were seventeen and eight respectively, and three on a spiny stellate cell; the interaction between a double bouquet cell and a postsynaptic pyramidal cell was mediated by ten synaptic junctions.

5. All three types of interneurone ($n = 6$; 2 for each type of cell) elicited short-latency IPSPs with fast rise time (10–90%; 2·59 ± 1·02 ms) and short duration (at half-amplitude, 15·82 ± 5·24 ms), similar to those mediated by $GABA_A$ receptors.

6. Average amplitudes of unitary IPSPs ($n = 6$) were 845 ± 796 μV (range, 134–2265 μV). Variability of IPSP amplitude was moderate, the average ratio of IPSP and baseline noise variance was 1·54 ± 0·96. High frequency activation of single presynaptic dendrite-targeting cells led to an initial summation followed by use-dependent depression of the averaged postsynaptic response. Double bouquet cell-evoked IPSPs, recorded in the soma, had a smaller amplitude than those evoked by the other two cell types. In all connections, transmission failures were rare or absent, particularly when mediated by a high number of release sites.

7. The results demonstrate that different types of neocortical GABAergic neurones innervate distinct domains on the surface of their postsynaptic target cells. Nevertheless, all three types of cell studied here elicit fast IPSPs and provide GABAergic input through multiple synaptic release sites with few, if any, failures of transmission.

On average, every fifth neurone and every sixth presynaptic terminal in the neocortex synthesizes and presumably releases GABA (Beaulieu & Somogyi, 1990). Synaptically released GABA is essential for limiting excitability within the cortex to operational levels, for maintaining the receptive field properties of neurones in the sensory cortex (Sillito, 1992), and it plays a critical role in the timing of both subthreshold events and the firing of cortical cells. Postsynaptic effects of GABA in the cortex are mediated by fast-activating anion channels, the $GABA_A$ receptors, and by $GABA_B$ receptors which activate a potassium conductance via a slower G-protein-mediated mechanism (Avoli, 1986; Connors, Malenka & Silva, 1988; Deisz & Prince, 1989; Benardo, 1994). There is general agreement that near the soma mainly $GABA_A$ receptors are activated, whereas GABA, iontophoretically applied to the dendrites, evokes complex multiphasic responses (Connors *et al.* 1988).

Most of the synaptically released GABA in the cortex originates from intrinsic cortical neurones, which differentiate into distinct cell types that appear to target different compartments of the postsynaptic neurone with their terminals (Somogyi, 1989). Although very few GABAergic neurones have been characterized quantitatively for their postsynaptic targets, it appears that, for example, cortical basket cells innervate the soma and proximal dendrites and are therefore likely to act through $GABA_A$ receptors. Neurones that innervate the dendritic domain of neocortical cells may also activate $GABA_A$ receptors (Connors *et al.* 1988; Thomson, West, Hahn & Deuchars, 1996). Furthermore, it has been suggested (Kang, Kaneko, Ohishi, Endo & Araki, 1994), mainly in analogy with results on hippocampal neurones (Newberry & Nicoll, 1985), that synaptically activated $GABA_B$ receptors are also located in the dendritic region. The action of GABA in the dendritic region is of interest because GABAergic mechanisms probably interact with other receptor-mediated events and voltage-dependent conductances specific to the dendritic region. Recently, microapplication of glutamate was used to evoke GABAergic responses from different sites in the cortex *in vitro* and the results suggested that $GABA_A$ and $GABA_B$ receptor-mediated responses can be evoked from different sites (Benardo, 1994). This finding was interpreted as indicating that separate neurones activate $GABA_A$ and $GABA_B$ receptors (Benardo, 1994), but the cells were not identified. In summary, although there is some information about the neuronal classes that release GABA and two major mechanisms of postsynaptic responses that have been found in cortical cells, until very recently only indirect experimental data linked some presynaptic cell types and postsynaptic mechanisms.

The identification of cortical neurones evoking particular postsynaptic effects can be made by recording simultaneously from both the presynaptic and postsynaptic neurones followed by microscopic visualization of the pre- and/or postsynaptic cells. Combining this method with subsequent electron microscopic verification of the synaptic junctions mediating synaptic interactions provides an opportunity for the rigorous assessment of differences and similarities in synaptic interactions (Gulyás, Miles, Sík, Tóth, Tamamaki & Freund, 1993; Buhl, Halasy & Somogyi, 1994; Deuchars & Thomson, 1995; Thomson *et al.* 1996). While the present paper was being reviewed, a detailed study (Thomson *et al.* 1996) in the rat parietal cortex showed that a heterogeneous group of interneurones evoked fast IPSPs in postsynaptic cells, some of which were pyramidal cells. In one case the five synapses mediating a fast IPSP were identified by electron microscopy on the proximal dendritic shafts of a pyramidal cell in layer V. A different interneurone that evoked a fast IPSP innervated both the dendrites and the somata of other neurones. Thus, the previously anatomically demonstrated synaptic diversity of cortical GABAergic neurones may not follow a diversity in postsynaptic receptor mechanisms, although pharmacological tests have not been carried out.

In order to quantify differences in the termination patterns of cortical GABAergic cells and to establish the precise placement of synapses that mediate identified postsynaptic effects we used paired intracellular recordings and subsequent light and electron microscopic analysis of the connections. Furthermore, we examined how the postsynaptic effect of identified GABAergic cells is influenced by the number of synapses between pairs of neurones and the location of synaptic release sites on the target cells. The visual cortex of the cat was chosen for this study because the laminar organization of its afferents and connections (Gilbert & Wiesel, 1979; Martin & Whitteridge, 1984), the contribution of GABAergic mechanisms to visual responses (Sillito, 1992) and the connections of GABAergic cells (Kisvarday, 1992) have been studied extensively. Some preliminary results from this study have been published in abstract form (Tamás, Buhl & Somogyi, 1995).

METHODS

Slice preparation

Adult female cats weighing 2·6–3·2 kg were deeply anaesthetized with an intramuscular injection of a mixture of ketamine (30 mg kg^{-1}) and xylazine (10 mg kg^{-1}). Following the cessation of noxious reflexes (pedal withdrawal and/or tail pinch reflex), a craniotomy was performed over the occipital cortex leaving the dura intact. After once more ensuring adequate levels of anaesthesia by ascertaining the loss of noxious pain reflexes (see above) the animals were immediately killed by intracardial perfusion with approximately 1·5 l of a modified (see below) artificial cerebrospinal fluid (ACSF) which was chilled and oxygenated. Following opening of the dura, a 5–8 mm thick block of the occipital cortex was excised in the frontal plane from both hemispheres and immersed in chilled ACSF. Using a vibroslice (Campden Instruments, Loughborough, UK) 400 μm thick sections were cut. The slices were trimmed, keeping only the crest of the lateral gyrus including areas 17 and 18, and transferred to a recording chamber, where they were maintained at 34–35 °C on a nylon mesh at the interface

between oxygenated ACSF and a humidified atmosphere saturated with 95% O_2–5% CO_2. The normal ACSF was composed of (mM): 126 NaCl, 3·0 KCl, 1·25 NaH_2PO_4, 24 $NaHCO_3$, 2·0 $MgSO_4$, 2·0 $CaCl_2$ and 10 glucose. During perfusion, cutting and pre-incubation all NaCl was replaced with equiosmolar sucrose (252 mM). The slices remained in the sucrose solution for 30 min before the perfusion medium was changed to normal ACSF.

Intracellular recordings and data analysis

Recording electrodes were pulled from standard wall borosilicate tubing, filled with 2% biocytin in 1·5 M KCH_3SO_4 and bevelled to a DC resistance of 80–150 MΩ. Putative GABAergic neurones were identified by their physiological characteristics, such as short-duration action potentials followed by large-amplitude fast after-hyperpolarizing potentials (fAHP). Once a stable recording had been obtained a search was made for cells displaying the electrophysiological properties of pyramidal and spiny stellate neurones (Fig. 2*D*). Capacitive coupling was eliminated on-line using a modified Axoprobe amplifier (Axon Instruments). Synaptic coupling was tested using on-line spike-triggered averaging whilst eliciting firing in the interneurone with either depolarizing current pulses or constant DC current injections. Firing rates in the interneurones were adjusted by varying the current intensity and, depending on the particular protocol, ranged between 0·3 Hz and > 100 Hz. Recordings were obtained with an Axoprobe amplifier which was operated in bridge mode. Experimental data were acquired using a PCM instrumentation recorder and stored on videotapes. Data analysis was continued off-line by (re)digitizing the data at 5–20 kHz using commercially available 12 bit A/D boards (RC Electronics Computerscope, Santa Barbara, CA, USA, and National Instruments Labmaster+, Newberry, UK) in conjunction with Axograph (Axon Instruments), RC Electronics Computerscope (RC Electronics) and WCP (courtesy of Dr J. Dempster, University of Strathclyde, UK) software packages. Unless indicated otherwise data are expressed as means ± S.D.

Resting membrane potentials were determined following electrode withdrawal and are given as the difference between surface DC potential and the steady state membrane potential without bias current injection. Membrane time constants were obtained from the decay of small hyperpolarizing current pulses fitting single exponential functions. The decay of the hyperpolarization back to baseline could be well fitted with a single exponential function in all cells. Likewise, input resistance was determined from measuring the maximal deflection of small hyperpolarizing current pulses. Spike amplitudes were taken from baseline to the peak of the action potential; spike duration was measured at half-amplitude. Unitary IPSP amplitudes were measured from baseline to peak. The corresponding noise levels were determined for the same time interval from baseline to baseline, using the pre-event interval of the same traces.

Histological processing and anatomical evaluation

In most of the cases, diffusion, presumably aided by depolarizing (0·1–0·5 nA) current pulses employed during recording, resulted in an adequate filling of neurones by biocytin. Slices were sandwiched between two Millipore filters to avoid deformations and fixed in 2·5% (w/v) paraformaldehyde, 1·25% (w/v) glutaraldehyde and 15% (v/v) saturated picric acid in 0·1 M phosphate buffer (pH 7·4) for 12–24 h. The tissue processing was based on previously described procedures (Buhl *et al.* 1994). Briefly, following gelatine embedding the slices were re-sectioned at a thickness of 60 μm and the biocytin-filled cells were visualized by the avidin-biotinylated horseradish peroxidase method with diaminobenzidine as chromogen. Sections were postfixed with 1% (w/v) OsO_4 and block stained in 1% (w/v) uranyl acetate, dehydrated and embedded into epoxy resin (Durcupan, Fluka) on glass slides.

Recovered cells were reconstructed from the serial 60 μm thick sections of the entire slice under a light microscope using a drawing tube at ×1250 magnification. Although cells can be filled completely, the reagents used for visualizing biocytin do not penetrate well into myelinated segments of axons, which often remain unstained. Nevertheless the axons can be followed accurately along the Ranvier nodes which are stained and easily recognised in osmium-treated material. The total number of axonal varicosities in the slice, some of them shown by subsequent electron microscopy to correspond to synaptic boutons, was counted during the drawing procedure. In each case, the location of the pre- and postsynaptic cell in the central portion of the slice enabled us to perform nearly full reconstructions of the dendritic arbors. The entire somato-dendritic surface of both recorded cells was tested for close appositions with filled axons, each of which was traced back to the parent soma. Light micrographs at different focal depth were taken from all of such close appositions and from characteristic axonal and dendritic patterns.

For the measurements of tissue volume occupied by the axonal arbors it was necessary to measure the potential changes in the volume of tissue from the living state in the animal to the epoxy resin embedded state. Several factors, probably acting in opposite directions, may influence changes in tissue volume, therefore the brain slices incubated *in vitro* are not comparable with perfusion-fixed brains even if identical histological procedures are used. While the tissue is sliced and kept in the chamber, cut processes and cells may die and shrink; other cells may become oedemic and there may be change in the extracellular space as well. Furthermore, the fixative is hyperosmotic and dehydration may result in some shrinkage although in osmium-fixed tissue this may not be large. To measure the final outcome of these influences three cats were mounted in a stereotaxic frame under ketamine and xylazine anaesthesia (as above) and an occipital craniotomy was made. A slit was made on the dura and a total of three pairs of parallel tracks, 1 mm apart, were made in the lateral gyrus. Glass capillaries of about 0·1 mm outer diameter, filled with 2 mg ml^{-1} biotinylated wheat germ agglutinin (WGA, Sigma) dissolved in ACSF, were used and oriented parallel with the sagittal plane and at about 20 deg to the horizontal plane. The capillaries were advanced from caudal to rostral about 7–8 mm in the cortex and while withdrawn, 6–10 nl of WGA solution was injected at every 0·5 mm. The WGA was visualized using the same histological procedure as for the intracellularly applied biocytin. The concentration of WGA proved to be too low for the 10–12 h survival time, and only a few cells showed granular labelling in their cell bodies around the injection tracks. Therefore, the capillary marks were mainly identified on the basis of the easily recognizable tracks of extravasated red blood cells visualized by the peroxidase reaction following fixation of the slices 10–12 h after the injection. Since the slices were cut in the frontal plane, the capillary tracks were sectioned nearly perpendicular and appeared as dots. Measurements of the distance between the tracks indicated an average of 6·0% increase relative to the intended distance. Comparison of thickness measurements of fresh slices and the processed and embedded sections indicated 2·1% collapse during the procedure and so the calculated overall volumetric change was an increase of 10·1%. The tissue volume containing the axonal arbors was calculated from two-dimensional drawings of each vibratome section by multiplying the area enclosed by a line connecting the consecutive, most distal tips of

Table 1. Postsynaptic target distribution of three classes of identified neocortical interneurones

Cell number		Postsynaptic targets (%) Soma	Dendritic shaft	Dendritic spine	Number of tested synapses*
Basket cells					
BC1	2104932	35·3	52·9	11·8	17
BC2	1102943	46·2	46·2	7·7	13
BC3	0812942	61·5	34·6	3·8	26
BC4	1102941	35·3	58·8	5·9	17
BC5	2402943c1t2	69·2	30·8	0·0	13
BC6	2402943c1	52·2	47·8	0·0	23
					Total 109
	Mean	49·9	45·2	4·9	
	S.D.	13·8	10·7	4·6	
Dendrite-targeting cells					
DTC1	1612941	4·2	83·3	12·5	24
DTC2	1412943	0·0	100·0	0·0	23
DTC3	0812944	7·7	80·8	11·5	26
DTC4	1506935	10·7	75·0	14·3	28
DTC5	0612944	0·0	82·4	17·6	17
					Total 118
	Mean	4·5	84·3	11·2	
	S.D.	4·7	9·4	6·7	
Double bouquet cells					
DBC1	1412942	0·0	36·0	64·0	25
DBC2	0812943	0·0	26·7	73·3	15
DBC3	2402943c2t2	0·0	32·3	67·7	31
DBC4	2402942	0·0	28·3	71·7	46
					Total 117
	Mean	0·0	30·8	69·2	
	S.D.	0·0	4·2	4·2	

* Random samples of electron microscopically identified postsynaptic elements.

axonal branches, with the thickness of the section measured in the light microscope at high magnification.

Following light microscopic analysis, axon-rich areas, including all layers covered by the axonal field, were cut out from the thin layer of resin on the slide and re-embedded for ultrathin sectioning. Serial sections were cut and mounted on single-slot Formvar-coated copper grids and stained with lead citrate. The sections were scanned in the electron microscope and all biocytin-filled axonal profiles were followed until they formed synaptic contacts. Since all profiles were followed and the plane of the section randomly cuts through the axonal branches, the above procedure ensured a random sample of postsynaptic targets. Each presynaptic terminal that was studied was examined completely in serial sections to establish the number of synapses it formed. Tracing of serial sections was also useful to distinguish between dendritic spines and small-calibre dendritic shafts as postsynaptic elements. In some cases, when the tracing was not feasible, small-diameter postsynaptic profiles containing mitochondria and/or microtubules were classified as dendritic shafts, although spines rarely contain mitochondria (authors' unpublished observations). Subsequently, all light microscopically detected sites of close appositions between filled axons and labelled somata, dendrites or spines were tested in serial electron microscopic sections. Although the identification of the postsynaptic specialization was not possible in some cases owing to the electron-opaque reaction end-product, we verified synaptic junctions based on the following criteria: (i) vesicle accumulation in the presynaptic axonal varicosity; and (ii) rigid membrane apposition between the pre- and postsynaptic element with a characteristic widening of the extracellular space. When the plane of the section was tangential to the junctional membranes, the synaptic cleft could be recognized by tilting the section using the goniometer of the electron microscope. Direct membrane apposition alone did not predict the presence of a synaptic junction (see e.g. Fig. 9*C*). Moreover, all filled somata were serially sectioned completely for electron microscopic analysis to check for the presence of axonal branches which may have been obscured by the opaque cell bodies.

Statistical methods

Interneurones were classified by cluster analysis based on random samples of their postsynaptic targets (Statistica for Windows, StatSoft, Tulsa, OK, USA). Joining trees were constructed by unweighted pair-group average (UPGMA; Sneath & Sokal, 1973) and Ward's (Ward, 1963) method of amalgamation and were based on Euclidean distances. Using the number of clusters given by this *a priori* cluster analysis we also performed *a posteriori* k-means clustering on the data. Furthermore, Fisher's exact test and

Pearson's χ^2 test for heterogeneity were applied to determine whether the cell groups defined by the cluster analysis were homogeneous and/or overlapping (S-Plus, Statistical Sciences, Seattle, WA, USA). The results obtained by the two tests were similar, although the P values were consistently higher using Fisher's test and we give the P values determined by this test. The non-parametric Mann–Whitney U test was applied to compare the properties of the different cell types. Unless indicated otherwise, results are given as means ± S.D.

RESULTS

Identification of interneurone subtypes

During physiological recordings neurones were tentatively identified according to their firing properties. Despite variability in the properties of distinct cell types, it must be emphasized that it was not possible to discriminate reliably between interneurones on the basis of physiological characteristics, therefore anatomical identification of cell types was essential. Some neocortical local-circuit neurones in the rat can be differentiated from others on the basis of their characteristic membrane and firing properties (Kawaguchi, 1995; Thomson *et al.* 1996). However, since several known interneurone classes were not represented in our sample, the qualitative properties used to detect interneurones may have biased our sample for the three classes presented here. The comparison of intrinsic membrane and firing properties of the different cell classes will require a more detailed analysis as shown in young rats (Kawaguchi, 1995). Since the primary aim of our study was to define the postsynaptic effects at known locations on the postsynaptic neurone, we used the postsynaptic target element pattern in the output of interneurones for classification, which is a good signature of a cell class. Nevertheless, even in the classes delineated by synaptic target patterns, only double bouquet cells appear to be homogeneous on the basis of axon location and dimensions; both basket cells (Somogyi, 1989; Kisvarday, 1992) and dendrite-targeting cells are heterogeneous.

After histological processing and light microscopic evaluation, fifteen cells that had largely aspiny dendrites were judged to have adequate axonal filling, suitable for complete reconstructions from the slices. In these cases, there were no partially or weakly filled axonal branches; all collaterals ended in fine terminal segments with varicosities, or were terminated by the slicing procedure at the surface of sections. Although the lateral and radial dimensions of axonal arborizations (530 ± 130 and 1050 ± 350 μm; $n = 15$) were greater than the slice thickness (390 ± 70 μm), primary and secondary axonal branches did not appear to have been cut during slicing, and only high order branches (0–37 per cell) reached the slice surface. All fifteen cells were processed for further electron microscopic analysis. A total of 344 efferent synapses, ranging from 13 to 46 for each cell, were collected and the proportions of the different postsynaptic elements were established. Axon terminals invariably established symmetrical, Gray's type II synaptic contacts on their postsynaptic targets.

We used the apparent heterogeneity in a random sample of the unlabelled postsynaptic target distribution to classify the recorded neurones (Fig. 1 and Table 1). Objective classification of interneurones was based on their unlabelled

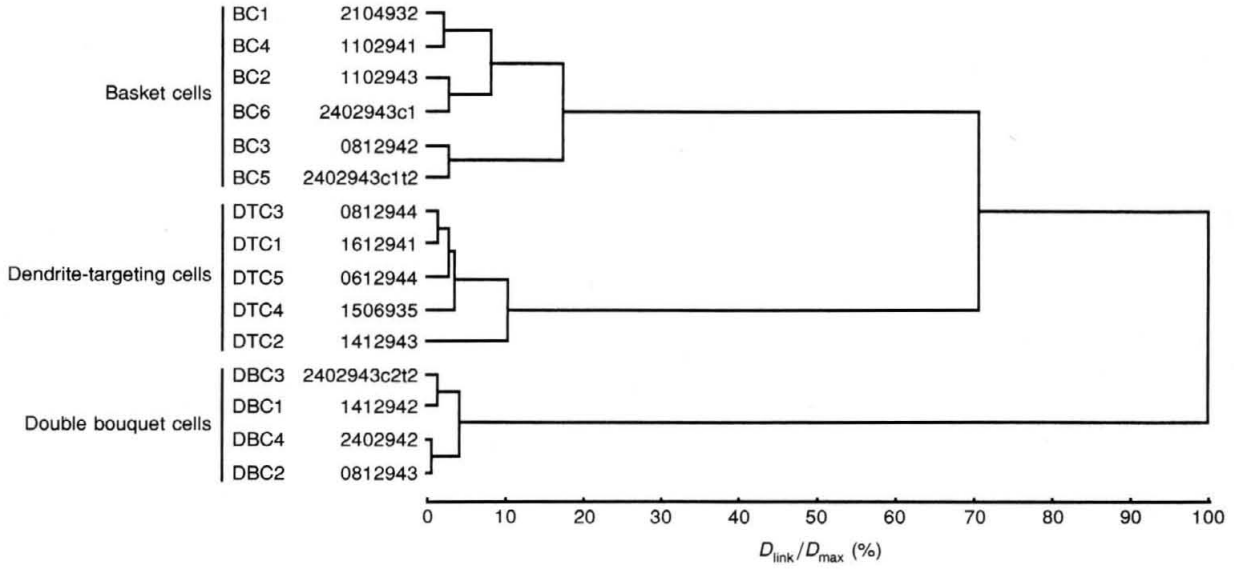

Figure 1. Cluster analysis of identified neocortical interneurones based on random samples of their postsynaptic targets

Interneurones were characterized on the basis of the distribution of their unlabelled postsynaptic targets (Table 1). A joining tree was calculated from cluster analysis using Ward's (Ward, 1963) method of amalgamation and Euclidean distances. Interneurones of the 3 clusters had somato-dendritic (basket cells), dendritic (dendrite-targeting cells) and spine (double bouquet cells) synaptic target preference. D_{link}, D_{max}: linking and maximal Euclidean distances.

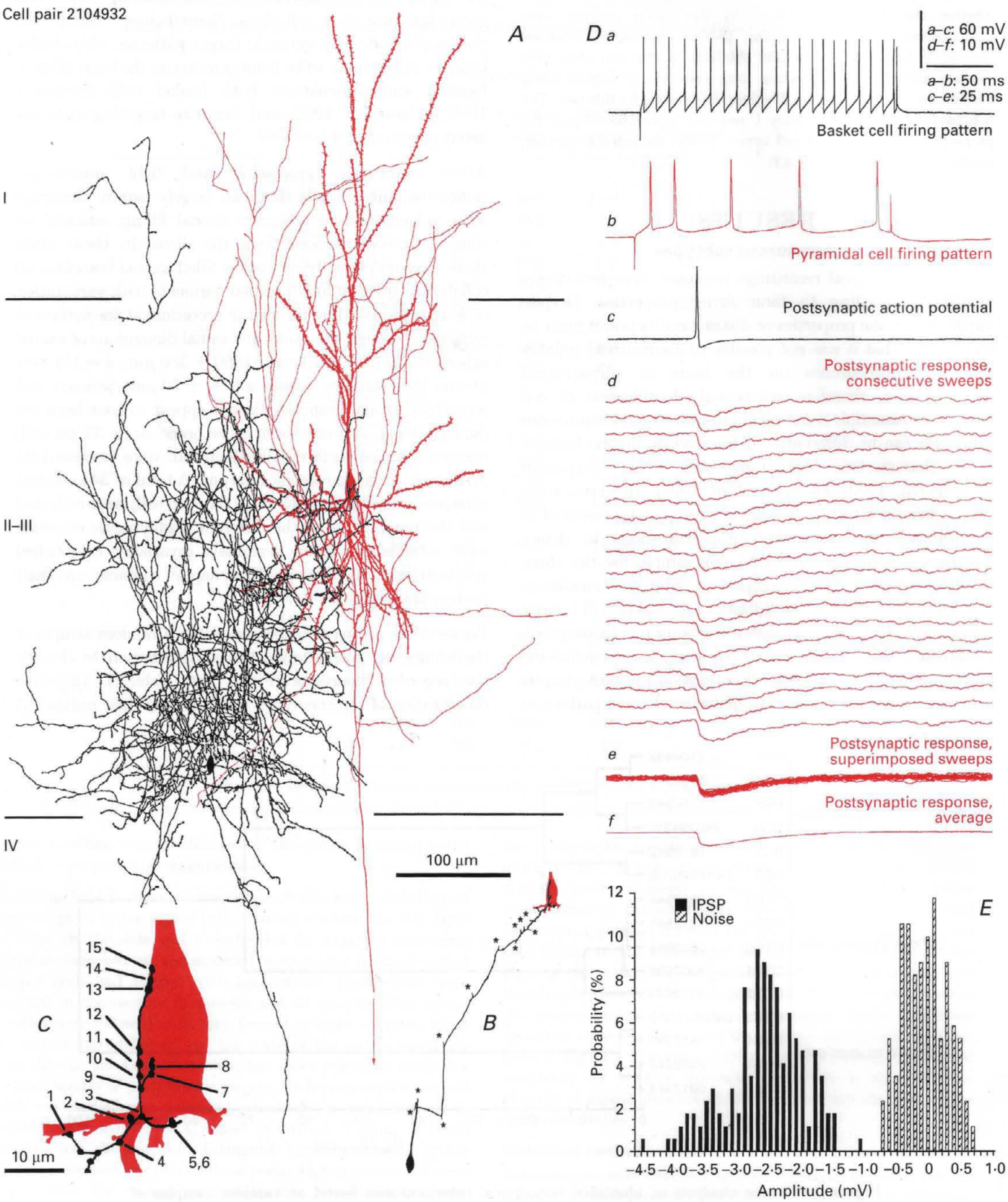

Figure 2. Light microscopic reconstruction and synaptic effect of a basket cell on a pyramidal cell in layers II–III of area 18

A, dendritic and axonal arborization of the postsynaptic pyramidal cell (red) and the presynaptic basket cell axon (black; dendrites were not recovered). *B*, route of the basket cell axon to synaptic boutons on the pyramidal cell. Branch points are indicated by asterisks. *C*, location of electron microscopically verified (see

postsynaptic targets. Joining tree clustering by unweighted pair-group average (Sneath & Sokal, 1973) and Ward's (Ward, 1963) method using Euclidean distances was performed. The two different amalgamation algorithms resulted in the separation of the same three cell groups on the constructed joining trees (Fig. 1). Interneurones of the three clusters had somato-dendritic, dendritic shaft or spine synaptic target preference. Thus, we defined the number of groups as three in the *a posteriori* k-means clustering of data. This reverse variance analysis grouped the same cells into each particular cluster, and proved that the groups differed significantly in postsynaptic elements (soma: $P < 0{\cdot}0003$; dendritic shaft: $P < 0{\cdot}0003$; dendritic spine: $P < 0{\cdot}0001$). The overall population of cells was heterogeneous with respect to the location of their terminals on postsynaptic neurones ($P < 0{\cdot}005$, Fisher's exact test), whereas groups of cells with somato-dendritic ($P < 0{\cdot}399$) or dendritic shaft ($P < 0{\cdot}343$) or dendritic spine ($P < 0{\cdot}960$) target preference were not significantly heterogeneous. Moreover, when we included *any* cell from a different group into a homogeneous class, heterogeneity became significant ($P < 0{\cdot}003$), showing that the groups were non-overlapping.

Thus, recorded neurones could be divided into three distinct and homogeneous groups based on their postsynaptic target distribution. (i) Neurones ($n = 6$) innervating heavily somata ($49{\cdot}9 \pm 13{\cdot}8\%$), dendritic shafts ($45{\cdot}2 \pm 10{\cdot}7\%$) and sometimes dendritic spines ($4{\cdot}9 \pm 4{\cdot}6\%$) were identified as *basket cells* (BC; Somogyi, Kisvarday, Martin & Whitteridge, 1983). (ii) A novel class of neocortical cells could be defined as *dendrite-targeting aspiny neurones* (DTC; $n = 5$) terminating predominantly on dendritic shafts ($84{\cdot}3 \pm 9{\cdot}4\%$) and less frequently on dendritic spines ($11{\cdot}2 \pm 6{\cdot}7\%$) and on somata ($4{\cdot}5 \pm 4{\cdot}7\%$). (iii) Neurones ($n = 4$) showing morphological characteristics of *double bouquet cells* (DBC; Somogyi & Cowey, 1981) preferred dendritic spines ($69{\cdot}2 \pm 4{\cdot}2\%$) to dendritic shafts ($30{\cdot}8 \pm 4{\cdot}2\%$) as postsynaptic elements and avoided somata.

Characteristics of smooth dendritic cells

The main parameters of the recorded cells are summarized for comparison in Table 2. The qualitative features that can be used to identify the three cell classes are summarized. Both the basket cell and the dendrite-targeting cell categories appeared heterogeneous in several features (see below).

Basket cells. Due to our sampling strategy, the recovered ($n = 6$) somata were restricted to layers II–III. The seven to eleven primary dendrites originated from the lower and upper poles of the cells. The smooth, strongly beaded secondary and tertiary dendrites rarely branched, were elongated radially, and most dendrites remained in layers II–III. Dendritic branching points occurred within about 40 μm from the perikaryon.

In most cases, the main axon collaterals were myelinated but they could be followed along the Ranvier nodes, due to the high contrast provided by the osmium treatment. Basket cell axons branched frequently at angles close to 90 deg and formed varicose terminal segments. Individual axonal branches did not produce dense basket-like configurations, but were frequently apposed to somata and proximal dendrites. Axonal varicosities of basket cells, tested by electron microscopy, invariably corresponded to synaptic boutons unevenly distributed (Table 2) in cortical layers. Cells BC1, BC2 and BC3 had dense, focal axonal arborizations overlapping with their dendritic tree and formed 97–100% of their boutons in layers II–III (Fig. 2). The axon of cells BC4, BC5 and BC6 sent descending collaterals to layers V and VI where 3–20% of their boutons were located, avoiding layer IV and establishing 76–91% of the axonal varicosities in layers II–III.

Basket cells had an average resting membrane potential of $-68{\cdot}6 \pm 7{\cdot}4$ mV ($n = 6$). Membrane time constant and input resistance were $6{\cdot}0 \pm 1{\cdot}9$ ms ($n = 3$) and $59{\cdot}0 \pm 11{\cdot}4$ MΩ, respectively. When it could be measured reliably ($n = 2$), basket cells had overshooting action potentials with amplitudes of 81·2 and 78·2 mV. Measured at half-amplitude, action potentials in these cases had a duration of 266 and 313 μs.

Dendrite-targeting cells. Their main characteristics were similar to basket cells, but the somata both in areas 17 and 18 were in layer IV (Figs 4 and 6). The seven to nine primary dendrites each divided into two to seven secondary and tertiary dendrites. Most of the dendritic branching points were located up to 40 μm from the soma. The strongly beaded, smooth individual dendrites formed two types of dendritic fields. Cells DTC1, DTC2 and DTC3 had spherical dendritic arborizations having radial and lateral

Fig. 3) synaptic junctions between the basket and pyramidal cells. Eleven synapses were found on the soma and 4 synapses on the most proximal basal dendrites, although most of the basal dendrites of the pyramidal cell were within the axonal cloud of the basket cell (see *A*). One bouton established two distinct synaptic release sites (5, 6; see Fig. 3). *Da* and *b*, the presynaptic basket cell fired non-accommodating trains of short-duration action potentials followed by a deep fast AHP in response to a 0·5 nA depolarizing current pulse, whereas the postsynaptic pyramidal cell responded with trains of accommodating and relatively broad action potentials, followed by a comparatively small fast AHP. *Dc* and *f*, action potentials (~1 Hz) of the basket cell resulted in a short latency, fast IPSP (average amplitude, $-2{\cdot}43 \pm 0{\cdot}60$ mV; monoexponential decay; $\tau = 18{\cdot}4$ ms) in the postsynaptic pyramidal cell, which was depolarized to −49 mV membrane potential. *Dd* and *e*, 20 consecutive sweeps illustrating the small variability of unitary IPSPs. *E*, the unitary IPSP amplitude distribution demonstrates the absence of response failures. $n = 170$ events.

Table 2. Parameters of three classes of smooth dendritic interneurone identified on the basis of their postsynaptic targets as established within the slices

	Basket cells			Dendrite-targeting cells ($n = 5$)		Double bouquet cells		
	n	Mean ± S.D.	Range	Mean ± S.D.	Range	n	Mean ± S.D.	Range
Soma diameter								
Radial (μm)	6	22 ± 5	15–30	23 ± 5	18–29	3	13 ± 3*	10–15
Lateral (μm)	6	20 ± 9	11–35	19 ± 3	15–23	3	8 ± 1	7–9
Dendritic tree diameter								
Radial (μm)	5	355 ± 30	304–372	504 ± 239	186–769	2	349 ± 86	288–410
Lateral (μm)	5	262 ± 27	234–301	340 ± 115	200–496	2	228 ± 40	200–256
Axon arborization diameter								
Radial (μm)	6	946 ± 232	677–1310	900 ± 397	497–1415	4	1414 ± 229	1245–1751
Lateral (μm)	6	568 ± 113	369–674	525 ± 153	259–639	4	489 ± 160	315–698
No. of axonal boutons	6	4442 ± 1212	2580–5685	3439 ± 543†	2991–4308	4	6171 ± 1964	5469–9048
No. of synapses per bouton	6	1·09 ± 0·08	1·00–1·18	1·39 ± 0·21†	1·14–1·64	4	1·03 ± 0·03	1·00–1·07
No. of synapses per cell	6	4866 ± 1481	2826–6427	4747 ± 819	3800–5870	4	6411 ± 2218	4805–9694
Volume of axonal arborization (mm^3)[1]	6	0·0192 ± 0·0064	0·0133–0·0312	0·0142 ± 0·004	0·0082–0·0176	4	0·0182 ± 0·0061	0·0129–0·0270
Efferent synapses per cell (1000 mm^{-3})	6	262 ± 74	161–352	354 ± 117	280–561	4	355 ± 57	295–431
Proportion of GABA synapses given by a cell (%)[2]	6	0·55 ± 0·15	0·34–0·73	0·74 ± 0·24	0·58–1·17	4	0·74 ± 0·12	0·62–0·90
On somata	6	2·10 ± 0·87‡	0·90–3·45	0·28 ± 0·31	0·00–0·69	4	0·00 ± 0·00	0·00–0·00
On dendritic shafts	6	0·42 ± 0·12	0·25–0·57	1·07 ± 0·35†	0·80–1·63	4	0·39 ± 0·07	0·34–0·50
On dendritic spines	6	0·11 ± 0·11	0·00–0·28	0·31 ± 0·19	0·00–0·51	4	1·94 ± 0·34*	1·49–2·30

[1]Calculated for slice; [2]calculated for the total volume occupied by the axon. * $P < 0·02$ relative to equivalent values of basket and dendrite targeting cells; † $P < 0·02$ relative to equivalent values of basket and double bouquet cells; ‡ $P < 0·01$ relative to equivalent values of dendrite targeting and double bouquet cells.

diameters of 350 ± 140 and 310 ± 100 μm, respectively, and the arbors were distributed mainly in layer IV (Fig. 4), and partly in layer III. Cells DTC4 and DTC5, which had radially elongated dendritic fields, had radial diameters of 770 and 710 μm and horizontal diameters of 500 and 280 μm, respectively. The radially oriented dendrites ran from the upper half of layer V to the middle of layer III.

The axon of dendrite-targeting cells originated from the upper (Figs 4 and 6) or the lower pole of the cell body, and almost immediately entered a myelin sheath which continued along the mainly radially oriented thick axonal trunks. Radial axonal trunks branched usually in acute angles and gave rise to short, necklace-like higher order axonal branches with large varicosities located in the neuropil. Dendrite-targeting cells had fewer boutons than basket or double bouquet cells, but their terminals established multiple synaptic release sites more often and, as a result, the three cell types established a similar mean number of synaptic junctions per cell (Table 2). The difference in dendritic patterns correlated with a difference in axonal arborizations amongst dendrite-targeting cells. The cells with spherical dendritic fields formed dense axonal clouds mainly in the same sublamina where the majority of dendrites were located. These axons branched frequently and formed dense plexus mainly in sublayer IVa (95 and 99% of the boutons of cells DTC3 and DTC2). In the case of cell DTC1, in addition to layer IVa (81%) small contributions were made to lower layer III (14%) and layers V and VI (6%). The two dendrite-targeting cells, having radially elongated dendritic fields, distributed their axons in a columnar manner, without particular laminar preference, although the largest proportion of the boutons was in layer IV (42 and 67% of cell DTC4 and DTC5). Comparing the axonal dimensions, both the radial spread (660 ± 270 μm *versus* 1415 and 1110 μm) and the volume (0·0131 ± 0·0047 mm^3 *versus* 0·0176 and 0·0144 mm^3) of the layer IV preferring axonal clouds was smaller than the two columnar axonal clouds.

Dendrite-targeting cells had an average resting membrane potential of −65·4 ± 8·38 mV ($n = 5$). When it could be measured reliably ($n = 4$), overshooting action potentials had an amplitude of 72·7 ± 11·3 mV. Measured at half-amplitude, action potentials had a duration of 264 ± 45 μs. Maximal firing frequency was 260 and 135 Hz in response to injecting a 1·5 nA, 200 ms depolarizing current pulse in cells DTC2 and DTC4 (Fig. 4*Ga*), and there was no significant spike frequency adaptation.

Double bouquet cells. Aspiny neurones with a high target preference for dendritic spines were recorded in layers II–III. The somata ($n = 3$) were slightly fusiform or conical in shape and were significantly smaller (Table 2) than those of basket and dendrite-targeting cells. Dendrites were recovered in two instances (cells DBC3 and DBC1) and were thin (< 1 μm), smooth and not beaded like those of the other two cell classes. Dendrites originated from the upper and lower pole of the perikaryon and branched infrequently, but unlike those of the other cell types, branching points could be observed up to 100 μm from the soma. The proximal dendrites of double bouquet cells frequently received asymmetrical synapses, which were invaginated into the dendritic shaft and surrounded by a large area of non-synaptic membrane apposition between the presynaptic terminal and the proximal dendrite. Such invaginated synapses could not be found on the soma or on more distal dendrites of double bouquet cells, or anywhere on basket and dendrite-targeting cells.

The characteristic bouton-studded, radial axonal bundles of double bouquet cells, traversing all layers, served for light microscopic identification (Somogyi & Cowey, 1981). Regardless of the incomplete recovery of the somata and dendrites, all axons were filled well from the initial segments to the terminal branches. The myelinated main axons branched after about 50 μm to unmyelinated, thin collaterals in a weeping willow-like manner. The higher order branches kept the radial orientation in layers I, IV, V and VI, but a

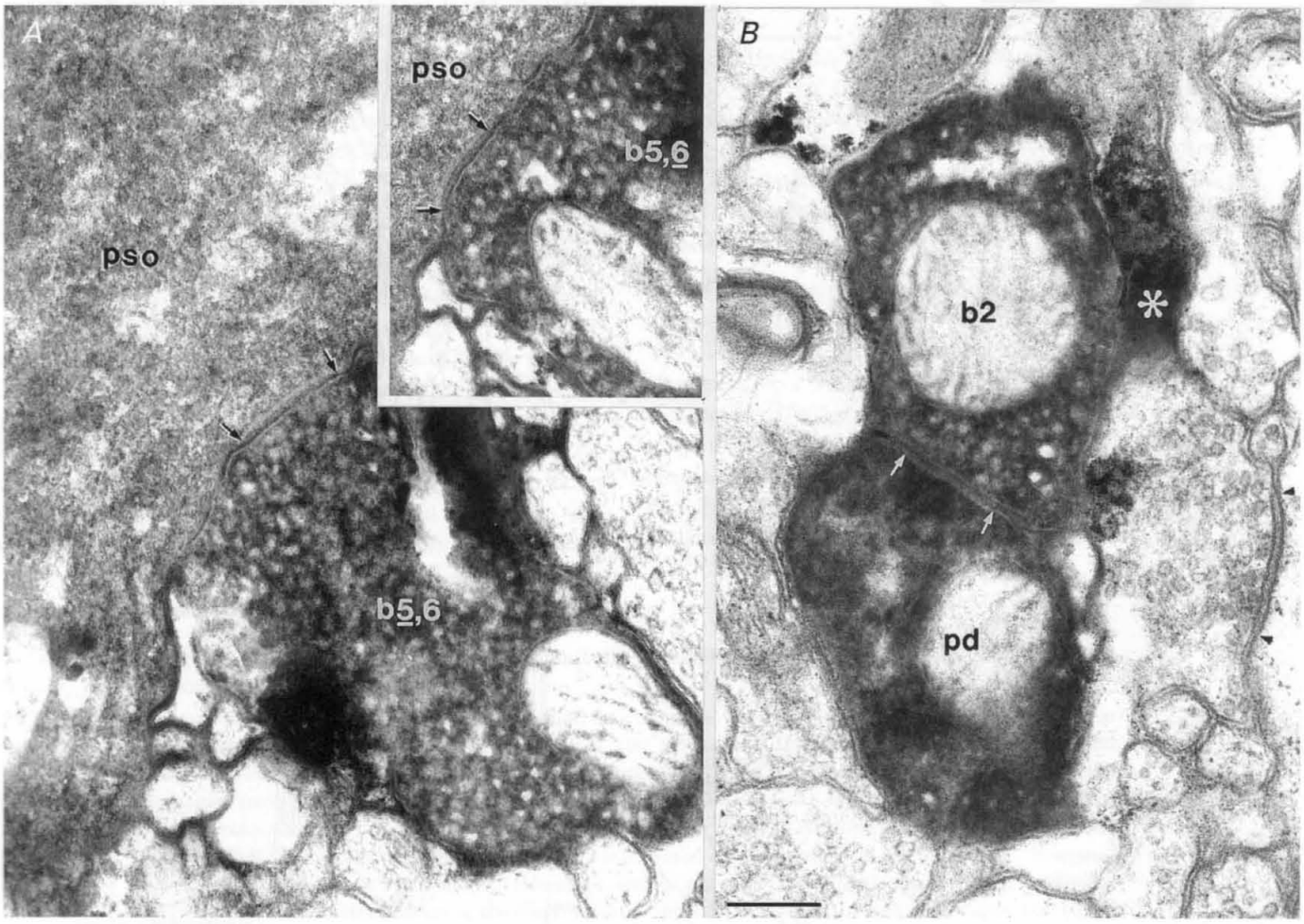

Figure 3. Electron microscopic evidence for synaptic junctions between the biocytin-filled basket cell terminals (numbering as in Fig. 2) and the pyramidal cell

A, a single bouton (b5,6) of the basket cell establishes two separate synaptic junctions (denoted as b5,6 and b5,6, respectively) on the pyramidal soma (pso), as shown from two serial sections. The synaptic active zones (between arrows) are defined by the rigid apposition of the plasma membranes and the widening of the extracellular space in the synaptic cleft. *B*, a bouton (b2) of the basket cell axon forms a synaptic junction (between arrows) on a pyramidal basal dendrite (pd). For comparison, a similar type 2 synaptic junction of unlabelled profiles is indicated (between arrowheads). The recorded and biocytin-filled processes of neurones are electron dense owing to the osmium treated peroxidase reaction product, which could spread slightly to neighbouring cellular profiles (e.g. asterisk) from very heavily filled terminals. The scale bar in *B* also applies to *A* and represents 0·2 μm.

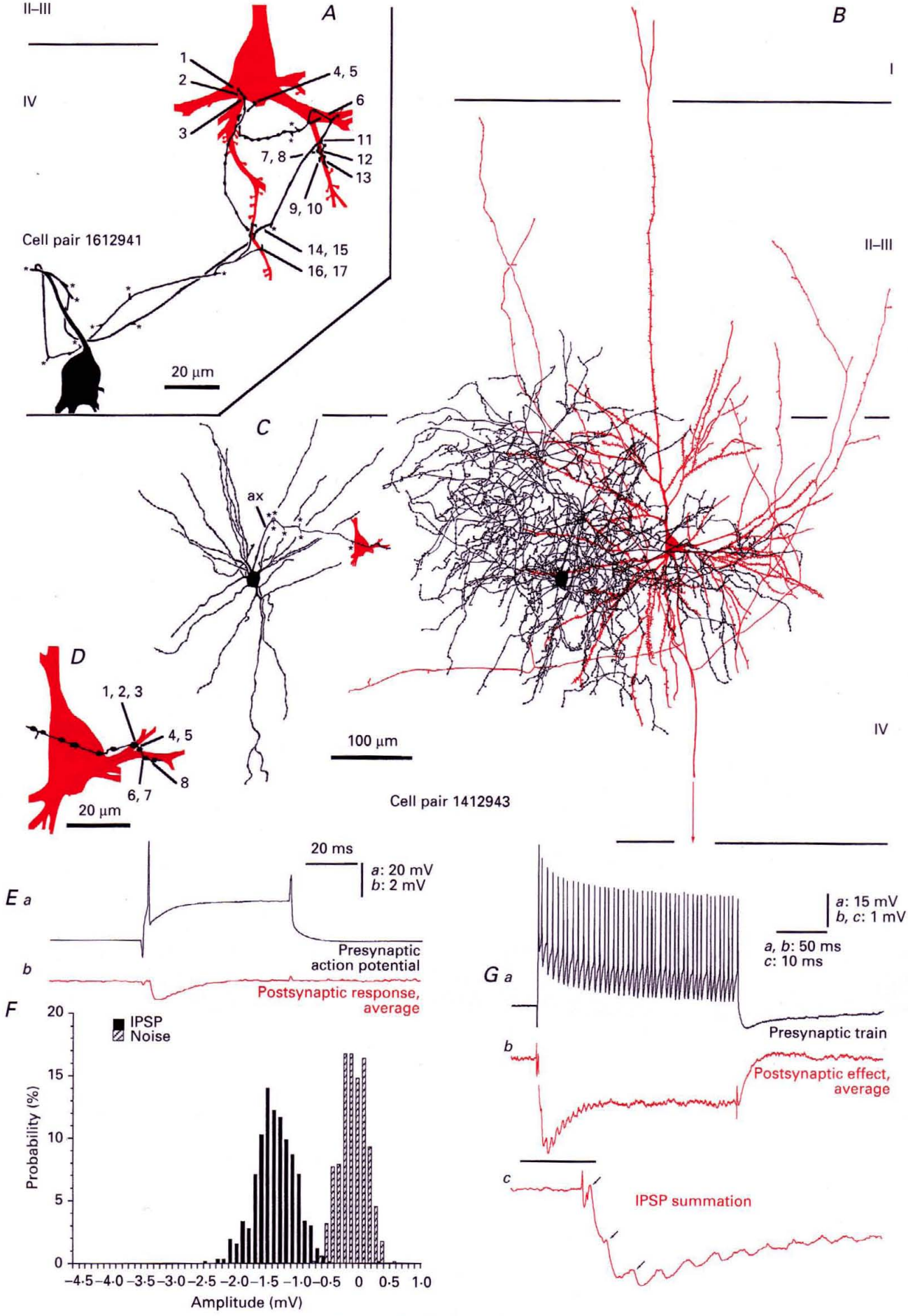

Figure 4. For legend see facing page.

substantial proportion of collaterals ran horizontally in layers II–III. The number of axonal thorn- or mushroom-like varicosities and synapses was the highest for this type of interneurone as a group. The laminar distribution of boutons showed a strong bias for layers II–III; 76 ± 6% of the varicosities were distributed in these layers, whereas layers I, IV, V and IV contained 8 ± 2, 10 ± 5, 2 ± 1 and 3 ± 2% of varicosities, respectively. The diameter of axonal arbors was much greater in layers II–III (490 ± 160 μm) than at the radial bundles measured in layer IV (65 ± 30 μm).

Double bouquet cells had an average resting membrane potential of −62·2 ± 2·6 mV ($n = 4$). Membrane time constants and input resistance values were 8·0 ± 3·3 ms and 56 ± 22·7 MΩ, respectively ($n = 3$). Three out of four double bouquet cells had non-overshooting action potentials with amplitudes of 60·1 ± 7·9 mV. Measured at half-amplitude, action potentials had a duration of 458 ± 129 μs. When calculating the difference in firing rate between the first and last interspike interval, the cells showed no apparent spike frequency adaptation, ranging from 55·8 to 140·3% with a mean of 108·6 ± 46·1%.

Neurones postsynaptic to identified GABAergic cells

The cell bodies of pyramidal cells ($n = 5$) were located in layers II–IV and had mean radial and lateral diameters of 26 ± 7 and 15 ± 6 μm. Four of the dendritic trees could be fully reconstructed, as the cell bodies were in the middle of the slice. Layers II–IV contain many different types of pyramidal cells (Gilbert & Wiesel, 1983; Martin & Whitteridge, 1984); the small number analysed here for their synaptic input does not warrant a detailed description of their features. Reconstructions of all four cells are presented in this and the accompanying paper (Buhl, Tamás, Szilágyi, Stricker, Paulsen & Somogyi, 1997), and so axonal and dendritic patterns can be compared with those of previously published cells. Cell 1412942 gave rise to a bifurcating apical dendrite characteristic for layer II pyramidal cells. The axons emitted collaterals mainly in layers II–III and V, then entered into a myelin sheath, usually near the border of the white matter. Although our preparations contained significant proportions of pyramidal axon arbors, published data (e.g. Gilbert & Wiesel, 1983) suggest that much of the axon may have been cut during the slicing procedure. Nevertheless, our specimens contained 453 ± 307 varicosities per pyramidal cell. The distribution of local pyramidal axons showed great variability, ranging from the narrow, columnar type comprised of radially oriented collaterals (e.g. cell 2104932) to a wider axonal tree composed of horizontally running branches (e.g. cell 1412943).

Pyramidal cells had an average resting membrane potential of −65 ± 12 mV ($n = 4$). Membrane time constant and input resistance were on average 13·6 ± 5·0 ms ($n = 3$) and 48·5 ± 26·9 MΩ ($n = 4$), respectively. Action potentials were overshooting with amplitudes of 77·0 ± 11·5 mV ($n = 3$). Measured at half-amplitude, action potentials had a duration of 790 ± 90 μs.

One of the postsynaptic neurones (cell 1506935) was a spiny stellate cell (Fig. 6). The triangular soma was located in layer IVa and had a radial and lateral diameter of 21 and 13 μm. Most of the dendritic branching points occurred at a distance of 20–65 μm from the perikaryon. The myelinated main axon emerged from the basis of the cell body and branched profusely in the middle of layer IV, forming straight, radially oriented branches which spanned the entire depth of the cortex, although most of the higher order

Figure 4. Two physiologically and anatomically identified dendrite-targeting cell to pyramidal cell connections in area 18

A, innervation of a layer III–IV border pyramid by a dendrite-targeting cell (shown as full reconstruction in Fig. 1 of the accompanying paper, Buhl *et al.* 1997). Although the electron microscopically verified synapses are clustered not only on the dendrites (nos 6–13; 14–17), but also on the basal part of the pyramidal soma (nos 1–5), the random sample of postsynaptic elements suggested that the presynaptic neurone was a dendrite-targeting cell. Some boutons made two separate synaptic junctions (numbers linked by comma). *B–G*, the other dendrite-targeting cell innervated a small pyramidal cell in layer IV. *B*, axonal pattern of the presynaptic cell (black) and dendritic and axonal arborization of the postsynaptic pyramidal cell (red). *C*, dendritic arborization of the dendrite-targeting cell (black) and the route of its axon (ax) to the pyramidal cell. Asterisks mark axonal branching points. *D*, a cluster of 4 boutons of the dendrite-targeting cell formed 8 separate synaptic junctions around a branching point of a basal dendrite. *E*, action potentials (~1 Hz) of the dendrite-targeting cell (*a*), evoked by a depolarizing current pulse, resulted in a short latency, fast IPSP (monoexponential decay; $\tau = 13{\cdot}3$ ms) with an average amplitude of −1·23 ± 0·32 mV in the postsynaptic pyramidal cell held at −51 mV membrane potential (*b*). *F*, amplitude distributions of IPSPs and baseline noise in the pyramidal cell. The segregation of IPSP and noise distributions demonstrates a highly reliable transmission. $n = 507$ events. *G*, summation and fading of IPSPs evoked by repetitive presynaptic firing. High frequency non-accommodating firing of the dendrite-targeting cell (*a*, single sweep) evoked by a depolarizing current pulse (1·5 nA), produced in the pyramidal cell the summation of the first 3 IPSPs (*b* and *c*, arrows; average of 9 sweeps), then the effect declined to a plateau at 47% of the peak amplitude. The monoexponential decay of the IPSP ($\tau = 11{\cdot}2$ ms) was similar to the decay of single action potential-evoked IPSPs. The time window shown expanded in *c* is indicated by bar in *b*.

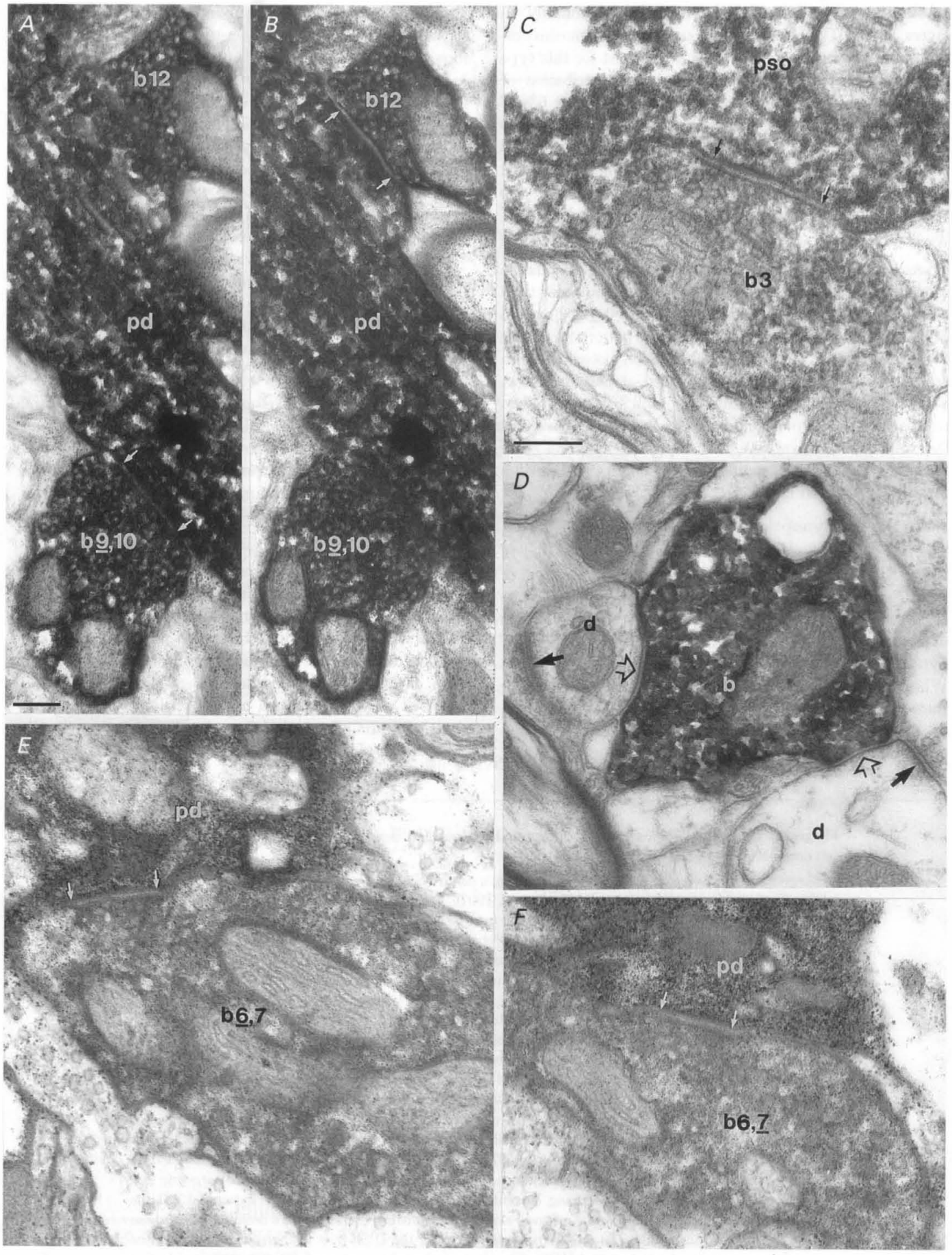

Figure 5. For legend see facing page.

Table 3. Relationship between light microscopically (LM) predicted and electron microscopically (EM) ascertained number and location of synaptic sites between identified pairs of synaptically coupled neurones

Cell pair	2104932			1612941			1412943			1506935			1412942		
Presynaptic	L. III BC			L. IV DTC			L. IV DTC			L. IV DTC			L. II–III DBC		
Postsynaptic	L. III PC			L. III–IV PC			L. IV PC			L. IV SSC			L. II PC		
Postsynaptic cell region	Soma	Den.	Spine	Soma	Den.	Spine	Soma	Den.	Spine	Soma	Den.	Spine	Soma	Den.	Spine
No. of close appositions (LM)	3	10	2	2	14	2	0	10	0	0	6	1	0	18	20
No. of membrane appositions (EM)	11	5	1	5	13	0	0	8	0	0	3	0	0	4	7
No. of presynaptic boutons (EM)	10	4	0	4	8	0	0	4	0	0	3	0	0	4	6
No. of synaptic junctions (EM)	11	4	0	5	12	0	0	8	0	0	3	0	0	4	6
Mean distance from the soma (μm)*	$1{\cdot}6 \pm 3{\cdot}7$			27 ± 21			11 ± 2			32 ± 4			76 ± 39		
Figures in present paper	Figs 2 & 3			Figs 4 & 5			Figs 4 & 5			Figs 6 & 7			Figs 8 & 9		
Figures in Buhl *et al.* 1997	—			Figs 1 & 2			—			—			Fig. 6		

*Estimated distance of verified synaptic junctions along the dendrites, showing the spatial segregation of innervation established by the three distinct classes of GABAergic cell. Den., dendritic shaft; L., layer; BC, basket cell; DTC, dendrite-targeting cell; DBC, double bouquet cell; PC, pyramidal cell; SSC, spiny stellate cell.

collaterals were in layers II–III. Within the slice the total number of boutons was 1190; layers II–III, IV, V and VI containing 67, 27, 4 and 2% of the varicosities. Some of the horizontal axonal branches in layer IV were truncated. The spiny stellate cell had a resting membrane potential of −61 mV. The membrane time constant and input resistance were 10·5 ms and 77 MΩ. The cell had overshooting action potentials of 68 mV in amplitude and 567 μs in duration, as measured at half-amplitude.

Placement of synaptic terminals in unitary, GABAergic cell to spiny cell connections

From six recorded unitary connections four allowed a full anatomical analysis; in the other two cases the postsynaptic neurones were not recovered (Table 3). In addition, a reciprocally connected dendrite-targeting cell to pyramidal cell pair (1612941, Table 3) was completely analysed anatomically, but in this case only the effect of the pyramidal cell was recorded (Buhl *et al.* 1997, accompanying paper).

A small basket cell (BC1) established a total of fifteen synaptic junctions with a pyramidal cell in layer III (Figs 2 and 3). The pyramidal cell was located at the edge of the basket cell axonal field. After twelve successive branching points, the axon reached the pyramidal cell to form the two 13th and two 14th order collaterals, which innervated the postsynaptic pyramidal cell (Fig. 2*B*). Eleven electron microscopically verified synaptic junctions were found on the soma and four on principal basal dendrites (Fig. 2*C*). One of the fourteen presynaptic boutons formed two separate synaptic junctions (Fig. 3*A*). The proportion of somatic synapses on the single identified pyramidal cell positioned at the periphery of the axonal field is similar to the random sample of unlabelled postsynaptic targets taken from various parts of the axonal arborization of this basket cell (Table 1).

Three unitary connections established by dendrite-targeting cells were analysed with correlated light and electron microscopy. Two pyramidal cells were innervated in a

Figure 5. Examples of electron microscopically verified synapses of the two dendrite-targeting cells shown in Fig. 4

A and *B*, two synaptic junctions (between arrows) on a pyramidal dendrite (pd) established by closely located boutons (b12; b9,10) from a cluster of the dendrite-targeting cell DTC1. In *A*, only one of the synaptic junctions established by bouton b9,10 is shown (synaptic contact number 9; the bouton here denoted as b9,10). Note that panels *A* and *B* show the same section but with a different tilting angle of the specimen to reveal the respective synaptic junctions (between white arrows) more clearly. *C*, a synaptic junction (between arrows) from the cluster on the pyramidal soma (pso) established by bouton b3 (cell DTC1). *D*, an axon terminal (b) of DTC3 forms synapses (open arrows) on two unlabelled dendrites (d) which also receive input from unlabelled boutons making asymmetrical synapses (arrows). *E* and *F*, a single large bouton (in the respective panels denoted as b6,7 and b6,7) of the dendrite-targeting cell DTC2 establishes two synaptic active zones on a dendrite of the pyramidal cell. The numbering of axon boutons is identical to that in Fig. 4. Scale bars, 0·2 μm; scale bar in *A* applies to *B* and *D*; scale bar in *C* applies to *E* and *F*.

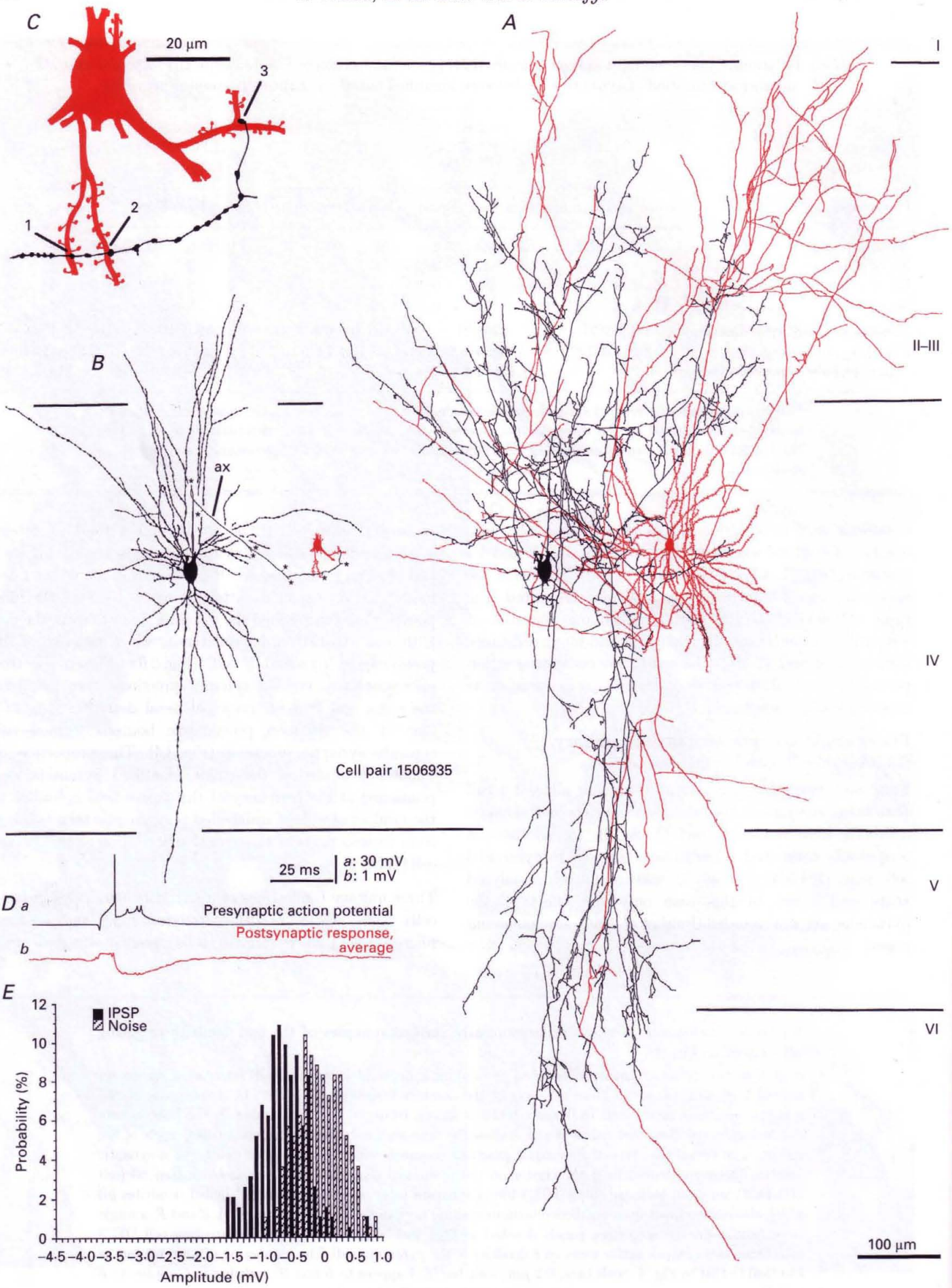

Figure 6. For legend see facing page.

similar, clustered manner by two different dendrite-targeting cells, having a dense axonal arborization in the sublayer IVa (Fig. 4). On the postsynaptic cells, these clusters of identified synapses were composed of four to eight closely placed synaptic release sites. In cell pair 1612941 (Fig. 4*A*), collaterals of two main axonal branches of the presynaptic cell formed three clusters of seventeen synapses on two basal dendritic shafts (nos 6–13; nos 14–17) and the basal pole of the soma (nos 1–5), at the site of the origin of a basal dendrite. In each case more than one higher order collateral converged on the same postsynaptic area (Fig. 4*A*). Five out of twelve boutons established two synaptic release sites (Fig. 5*A–C*). In cell pair 1412943 an 8th order branch of the presynaptic dendrite-targeting cell established a cluster of synapses composed of eight synaptic release sites next to a branching point of a basal dendritic shaft (Fig. 4*B–D*). All but one of these four boutons formed more than one synaptic junction (Figs 4*D* and 5*E* and *F*).

In layer IV, one presynaptic dendrite-targeting cell (DTC4) having the axon in layers III–VI innervated a spiny stellate cell (Fig. 6). A 7th order branch of the presynaptic axon formed two synapses on dendritic shafts, then, after two additional bifurcations, the axon terminated on a branching point of a different dendrite of the spiny stellate cell. The three synapses were established by three boutons (Fig. 7) and were equidistant (32·0 ± 3·7 μm) from the soma of the postsynaptic cell.

The light and electron microscopically analysed double bouquet cell to pyramidal cell pair (DBC1, 1412942, Fig. 8*A–E*) was reciprocally coupled. Details of the pyramid-to-double bouquet cell connection are presented in the accompanying paper (Buhl *et al.* 1997). Numerous collaterals of the double bouquet cell crossed the pyramidal cell dendrites and appeared to be in direct contact at thirty-six sites with different parts of the postsynaptic cell. *All* of these apparent contacts were examined electron microscopically, but only some of them were found to be synaptic sites. Eight different high order branches of the double bouquet cell axon innervated the pyramidal cell and established six synaptic junctions on dendritic spines and four on dendritic shafts (Fig. 8*C*). The synapses were widely distributed in terms of distance from the soma, but the ten synapses were on six dendritic branches originating from only three main dendrites. In two cases, both a dendritic spine and also the parent dendritic shaft received input from the same axon branch of the double bouquet cell (synapses nos 2,1 and 9,8). None of the ten presynaptic boutons formed more than one synaptic junction either on the pyramidal cell or on neighbouring unlabelled postsynaptic targets (Fig. 9). In the case of the other double bouquet cell (DBC2) to pyramidal cell pair (0812943) the postsynaptic neurone could be identified, but since the bulk of the dendritic tree disintegrated, the location of the synaptic junctions mediating the synaptic interaction could not be established (Fig. 8*F*).

Kinetics of unitary IPSPs

In the six paired recordings, two presynaptic basket cells, two dendrite-targeting cells and two double bouquet cells elicited unitary IPSPs in five postsynaptic pyramidal cells and one spiny stellate cell. All three cell types evoked short-latency (< 1·5 ms) IPSPs, with rise and decay kinetics similar to $GABA_A$ receptor-mediated synaptic potentials (Figs 2*D*, 4*E* and *G*, 6*D*, 8*D* and *G*). Reversal potentials, indicating that probably chloride was the major charge carrier, were −63·3 mV for basket cell BC2 and −67·6 mV for double bouquet cell DBC1, as extrapolated from hyperpolarizing IPSPs measured at membrane potentials ranging from −58 to −33 mV and −59 to −44 mV, respectively. The decay phase of all six unitary IPSPs could be adequately fitted with a single exponential function, with time constants between 9·1 and 18·1 ms. Similarly, single exponentials could be fitted to the decay phase of averaged small (0·1 nA) current pulses injected through the recording electrode into the postsynaptic cell bodies (the impalement site could be recognized after the recovery of the cells). In the neurones postsynaptic to the same basket and dendrite-targeting cells, unitary IPSPs had decay time constants (104 ± 8%) similar to the respective somatically delivered current pulses, whereas double bouquet cell-evoked IPSPs decayed more slowly, their time constants being 232 ± 57% of that of intrasomatic current pulses. Unitary IPSP conductance could only be calculated for one of the double bouquet cell (DBC1)-evoked IPSPs (for method see Benardo, 1994), and was 301 pS.

Figure 6. Reconstruction and synaptic effect of a dendrite-targeting cell on a spiny stellate cell in area 17

A, axonal pattern of the presynaptic dendrite-targeting cell (black) and dendritic and axonal arborization of a postsynaptic spiny stellate cell (red). *B*, dendritic arborization of the dendrite-targeting cell and its axonal branch (ax) contacting the spiny stellate cell; axon branching points are indicated by asterisks. *C*, synaptic boutons (1–3) on the spiny stellate are equidistant from the soma. *D*, action potentials (~1 Hz) of the dendrite-targeting cell evoked by current injection (*a*, averaged) resulted in a short latency, fast IPSP (monoexponential decay, $\tau = 10{\cdot}5$ ms) with an average amplitude of −0·61 ± 0·42 mV in the postsynaptic cell held at a membrane potential of −61 mV (*b*, average of 193 sweeps). *E*, amplitude distributions of IPSPs and baseline noise in the spiny stellate cell. The overlap of IPSP and noise distributions reflects the small amplitude of the IPSP evoked by 3 synaptic junctions. Note the lack of a distinct peak of IPSPs at 0 mV. $n = 193$ events.

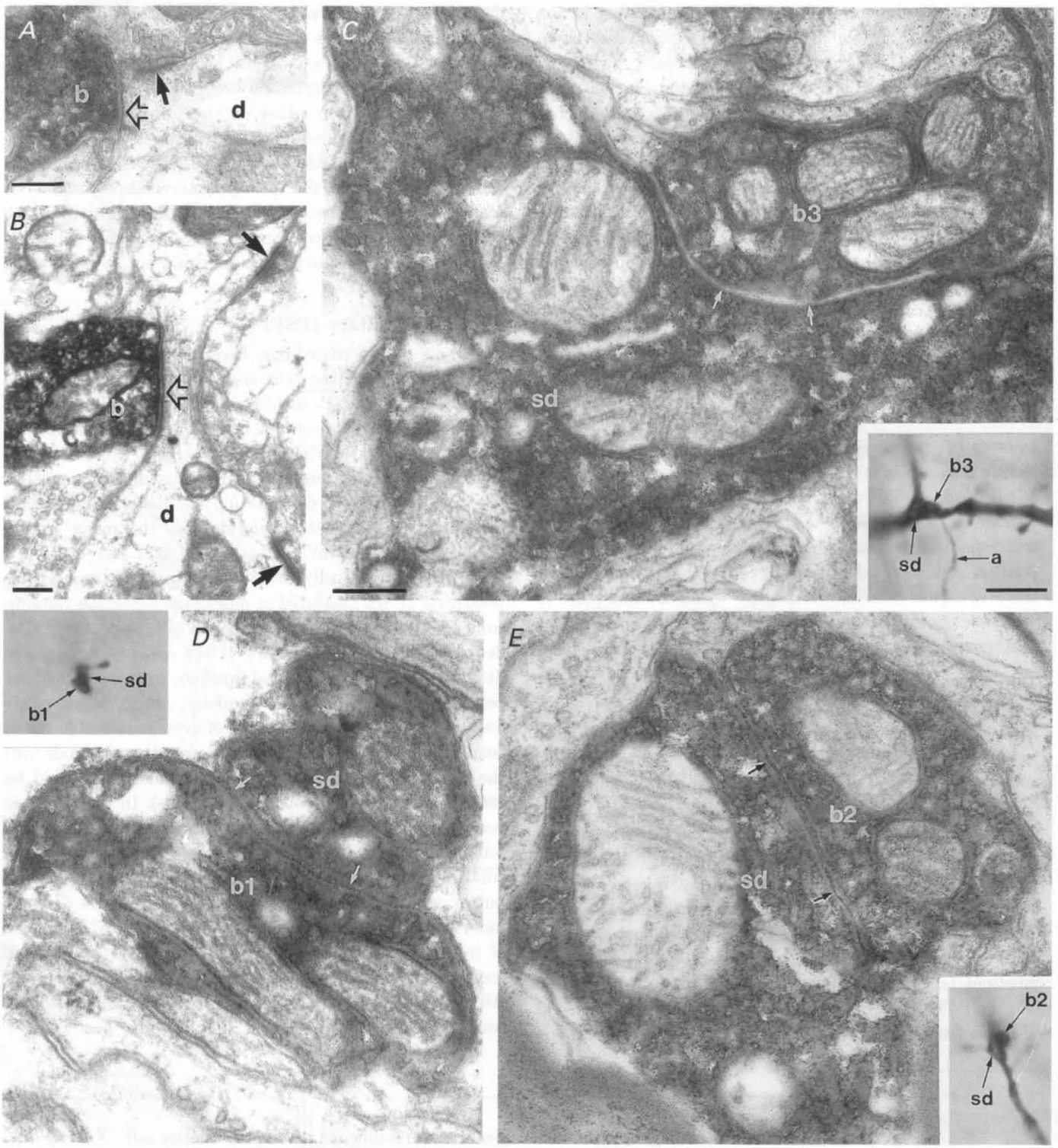

Figure 7. Electron microscopically verified synapses of the dendrite-targeting cell on the spiny stellate cell shown in Fig. 6

A and *B*, an axon terminal of the dendrite-targeting cell (b) forms synapses (open arrows) with unidentified dendrites (d) next to asymmetrical synapses (arrows). The dendrite (d) in *B* is beaded and is characteristic of GABAergic cells. *C–E*, correlated light (insets) and electron micrographs of the identified synaptic contacts between the dendrite-targeting cell and the spiny stellate cell. Each of the three boutons (b1, b2, b3) formed one synaptic junction (between arrows) on the postsynaptic spiny stellate dendrites (sd). In the inset of *C*, the axon (a) of the dendrite-targeting cell is apparent. Scale bars, 0·2 μm; inset: 5 μm; scale bars in *C* also apply to *D* and *E*.

Average IPSP amplitudes were 845 ± 797 μV and ranged from 131 to 2265 μV in the postsynaptic cells. Basket cells BC1 and BC2 elicited IPSPs with an average amplitude of 2265 μV (Fig. 2*Df*) and 372 μV at membrane potentials of −49 and −55 mV in the postsynaptic pyramidal cells. These events had 10–90% rise times of 1·9 and 1·7 ms and, measured at half-amplitude, a duration of 20·6 and 6·9 ms. Unitary IPSPs elicited by dendrite-targeting cells DTC2 and DTC4 had average amplitudes of 1222 and 763 μV (mean, 992·5 μV) at a membrane potential of −51 and −61 mV in the postsynaptic pyramidal and spiny stellate cells. Dendrite-targeting cell-evoked events had a 10–90% rise time of 1·6 and 3·1 ms and a duration at half-amplitude of 13·4 and 23·3 ms. Double bouquet cells DBC2 and DBC1 elicited IPSPs in the postsynaptic pyramidal cells with average amplitudes of 134 and 443 μV (mean, 288·5 μV) at membrane potentials of −51 and −48 mV. These events had a 10–90% rise time of 4·3 and 2·7 ms and a duration at half-amplitude of 10·4 and 16·2 ms.

Unitary IPSP summation and use-dependent depression

The postsynaptic effect of high frequency trains of presynaptic action potentials were tested in three pairs of neurones. The compound IPSPs elicited by dendrite-targeting cells DTC2 and DTC4 were similar and initially summated in the postsynaptic pyramidal and spiny stellate cells (e.g. Fig. 4*G*). The initial three to four IPSPs approximately doubled the amplitude of single action potential-evoked events. The first action potential resulted in the largest amplitude increase of the IPSP, whereas successive events gradually added less and less to the amplitude of the IPSP. Although the presynaptic firing frequency remained constant, the response gradually declined to a stationary level around half of the maximum of the summated amplitude. In the case of the tested double bouquet cell DBC1 to pyramidal cell pair (Fig. 8*Dc–e*), IPSP summation was relatively weak due to the long interspike intervals of the presynaptic tetanus and the rapid IPSP decay, a consequence of a relatively fast membrane decay time constant. Although the decay time constants of compound IPSPs elicited by trains of presynaptic action potentials could not be measured reliably due to the limited number of sweeps or the apparent overshoot in the response (DTC2, Fig. 4*G*), the decay back to baseline did not appear to be prolonged relative to the single action potential-evoked events.

Amplitude distribution of unitary IPSPs

The amplitudes of unitary IPSPs fluctuated to some degree at each interaction tested, although a significant portion of this variability may have originated from the recording noise. Superimposition of successive events already revealed the apparent absence of transmission failures and showed that the amplitude of individual events fluctuated around the average of the postsynaptic response (Fig. 2*D*). For further analysis, amplitude histograms of unitary IPSPs and the corresponding baseline noise were compared (Figs 2*E*, 4*F*, 6*E* and 8*E*) for those cases where the number and location of synaptic junctions between the pre- and postsynaptic cells had been determined. In all four interactions tested, the variance of IPSP amplitudes exceeded that of the baseline noise, as their ratio ranged from 1·1 to 3·1 (mean ± S.D., 1·5 ± 1·0). The overlap between the signal and noise distributions decreased with the increasing number of synaptic junctions mediating the events, with the absence of such overlap indicating the complete absence of transmission failures in the connections mediated by eight and fifteen release sites originating from the dendrite-targeting cell DTC2 and the basket cell BC1 (Figs 2 and 4). Moreover, the absence of a distinct peak around the zero amplitude level suggests few, if any, response failures in the connections mediated either by the few synapses (3) established by dendrite-targeting cell DTC4, or by the more distally placed release sites formed by double bouquet cell DBC1 (Figs 6 and 8).

DISCUSSION

Interneurones subdivide the surface of postsynaptic cells

The differentiation of multiple types of GABAergic cortical cells and the precise segregated placement of their efferent synapses strongly suggest that inhibition does not act non-specifically and globally, but instead a highly constrained network of GABAergic cells evolved to control functionally distinct domains of pyramidal cells presumably through $GABA_A$ receptors. The input domain (dendrites) is regulated by double bouquet and dendrite-targeting cells, possibly in an input pathway-specific manner, the final integration domain (soma) is regulated by basket cells and the output domain (axon initial segment) is controlled by the axo-axonic cells (Somogyi, 1989). Most of the GABAergic influence examined here is intracolumnar, in the tangential plane within 200 μm of the parent cell, and is highest in the vicinity of the cell body, in contrast to large basket cells that have long tangentially projecting axons (Kisvarday, 1992) suitable for intercolumnar interactions.

The characteristic postsynaptic target distribution of single interneurones is apparent both in the overall randomly taken target sample and in the location of synapses between identified pairs of synaptically coupled cells. The result of such a comparison suggests that the distribution of synapses on a particular postsynaptic cell is optimized for that particular input and the degree of variability in the placement of synapses on the target cell population is small. An apparent exception to this synaptic organizational rule is the innervation of a pyramidal cell body by a higher proportion (30%) of boutons of a dendrite-targeting cell, in comparison with its overall target pattern (4%). However, the somatic GABAergic synapses were close to the origin of a major dendrite which could have been the preferentially influenced part of the cell, resulting in the clustering of somatic synapses.

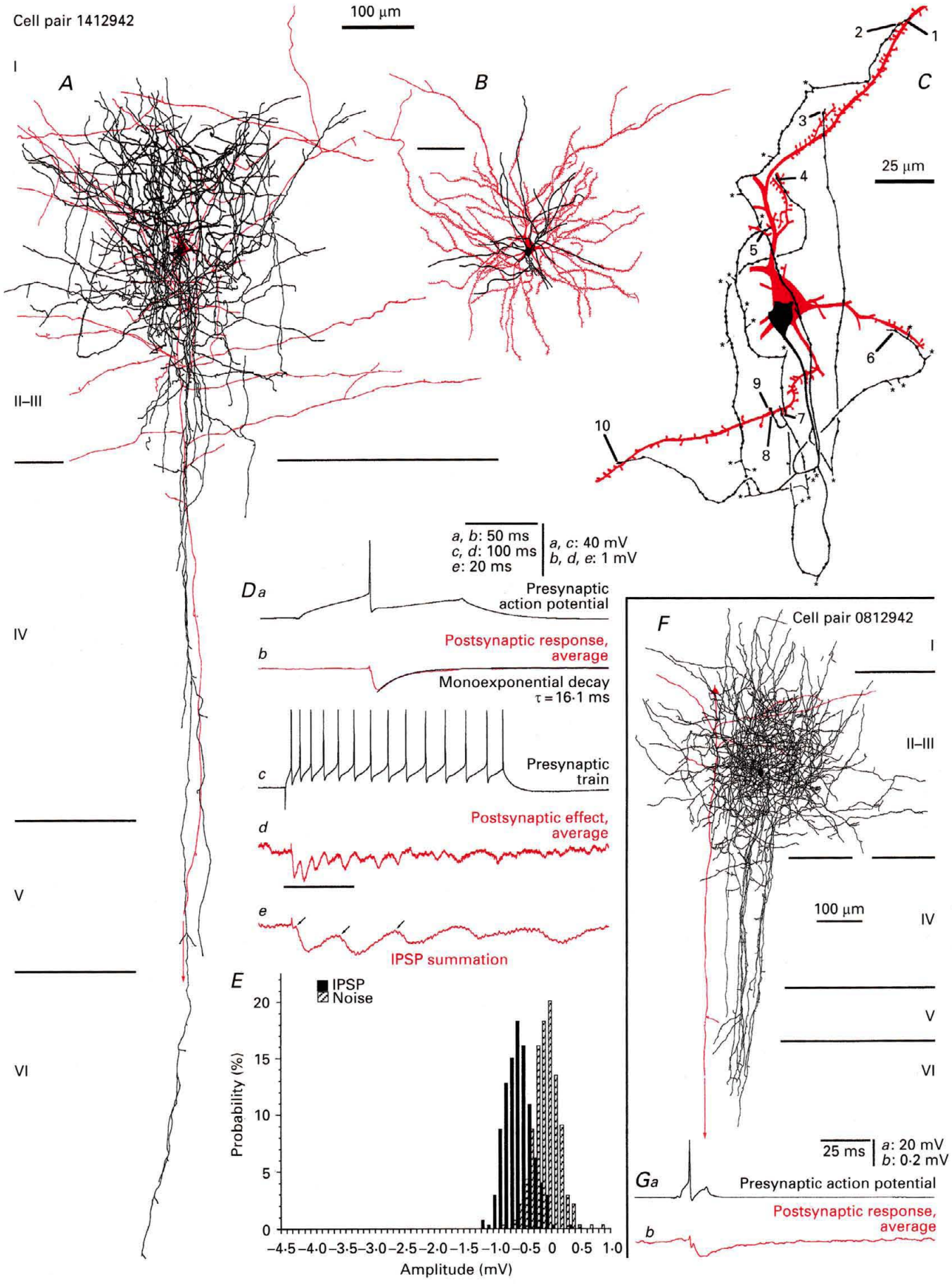

Figure 8. For legend see facing page.

It is unlikely that basket, dendrite-targeting and double bouquet cells innervate separate populations of spiny cells, because the pyramidal cells that were innervated on proximal dendrites by identified dendrite-targeting cells also received unlabelled synapses on their somata, which were probably supplied by basket cells. Similarly, the cell body of the intracellularly labelled pyramidal cell, which was the recipient of the double bouquet cell synapses, was also innervated by many boutons. Although it is possible that different classes of cortical spiny cells differ in the complement of their presynaptic GABAergic interneurone types, at present the most parsimonious hypothesis is that the three types of GABAergic cell studied here converge on several classes of postsynaptic spiny cells. Furthermore, in the cat visual cortex GABAergic axo-axonic cells innervate exclusively the axon initial segment, and additional types of GABAergic cell, such as the neurogliaform cell, contribute to dendritic innervation (Somogyi, 1989).

The results on the synaptic target distribution of double bouquet cells show considerably higher proportions of spines than previous studies using Golgi-impregnated cells in the cat (Somogyi & Cowey, 1981) or calbindin- and tachykinin-immunoreactive neurones in the monkey (DeFelipe, Hendry, Hashikawa, Molinari & Jones, 1990). The previous studies revealed a much smaller tangential extent of the axon in the superficial layers because in the studied specimens it was not possible to follow individual axons over large distances. Consequently, they may not have been fully representative of the overall synaptic target pattern. In Golgi-impregnated and immunostained material the sampling of axons belonging to single identified cells is more difficult than in the material used here. Finally, the double bouquet cell class may be heterogeneous with respect of synaptic target preference.

In spite of the overall segregation of GABAergic innervation, partial overlap on the surface of the postsynaptic cell originating from distinct sources is likely. For example, proximal dendrites may represent a common termination zone for basket as well as dendrite-targeting cells. Similarly, although most of the synapses made by the double bouquet cell on a pyramidal cell were more distal than those given by dendrite-targeting cells to other pyramidal cells, some overlap in the innervated zones is possible. A remarkable feature observed in the innervation pattern of dendrite-targeting cells is the clustering of presynaptic terminals on small areas of the postsynaptic dendritic surface. This arrangement raises the possibility that some GABAergic inputs are associated with some other input to the same individual dendrite as hypothesized earlier (Somogyi, 1989). A similar co-association of excitatory and inhibitory inputs is also suggested by the dual inputs to single dendritic spines from the GABAergic double bouquet cells and as yet unidentified terminals making type I synapses.

Fast IPSPs are evoked on segregated subcellular domains of cortical spiny cells

Unitary IPSPs evoked by basket, dendrite-targeting and double bouquet cells have fast kinetics and a relatively fast, monoexponential decay with an extrapolated reversal potential around the predicted chloride equilibrium potential. Even the slowest postsynaptic events, i.e. those evoked by double bouquet cells, had a time to peak and decay much shorter than those mediated by pharmacologically isolated IPSPs mediated by $GABA_B$ receptors (Benardo, 1994). Although we have not obtained pharmacological evidence, the similarity of the above properties to those reported earlier for $GABA_A$ receptor-evoked responses (Avoli, 1986; Connors *et al.* 1988; Deisz & Prince, 1989; Benardo, 1994; Deuchars & Thomson, 1995) strongly suggests that the postsynaptic action of these types of interneurone is mediated by $GABA_A$ receptors. The similarity in decay time constants between somatically delivered hyperpolarizing current pulses and unitary IPSPs evoked by basket and dendrite-targeting cells indicates that the decay of fast

Figure 8. Reconstructions and synaptic effects of double bouquet cells on pyramidal cells

Axonal (*A*) and dendritic (*B*) arborizations of a reciprocally connected double bouquet cell (black) and pyramidal cell (red) pair in area 18. *C*, innervation of the pyramidal cell by the double bouquet cell showing only the connected processes and cell bodies. Six electron microscopically verified synapses were on dendritic spines (2, 3, 5, 7, 9, 10) and four on dendritic shafts (1, 4, 6, 8) at various electrotonic distances from the soma. The branching points of the axon are labelled by asterisks. The distance between the double bouquet and pyramidal cell bodies was 35 μm in depth. *D*, action potentials (~2 Hz) of the double bouquet cell evoked by current injection (*a*, average) resulted in a short latency, fast rising IPSP, with an average amplitude of $-0{\cdot}44 \pm 0{\cdot}23$ mV in the postsynaptic pyramidal cell held at a membrane potential of −48 mV (*b*, average of 273 sweeps). At the injection of a 0·4 nA depolarizing current pulse, the double bouquet cell fired accommodating trains of short-duration action potentials (*c*) which evoked postsynaptic IPSPs of decreasing amplitude (*d*). Only the first 2 IPSPs summated moderately (*e*). The time window shown in *e* is indicated by the bar in *d*. *E*, amplitude distributions of IPSPs and baseline noise in the pyramidal cell. Note the lack of a distinct peak of IPSPs at 0 mV indicating the lack of response failures. $n = 273$ events. *F*, reconstruction of another double bouquet cell (black) to pyramidal cell (red) pair of synaptically coupled neurones. Dendrites of the pyramidal cell were not recovered. *G*, action potentials (~2 Hz) of the double bouquet cell evoked by current injection (*a*, averaged) resulted in a short latency, fast rising IPSP (monoexponential decay, $\tau = 14{\cdot}7$ ms) with an average amplitude of −0·13 mV in the postsynaptic pyramidal cell, held at a membrane potential of −51 mV (*b*, average of 520 sweeps).

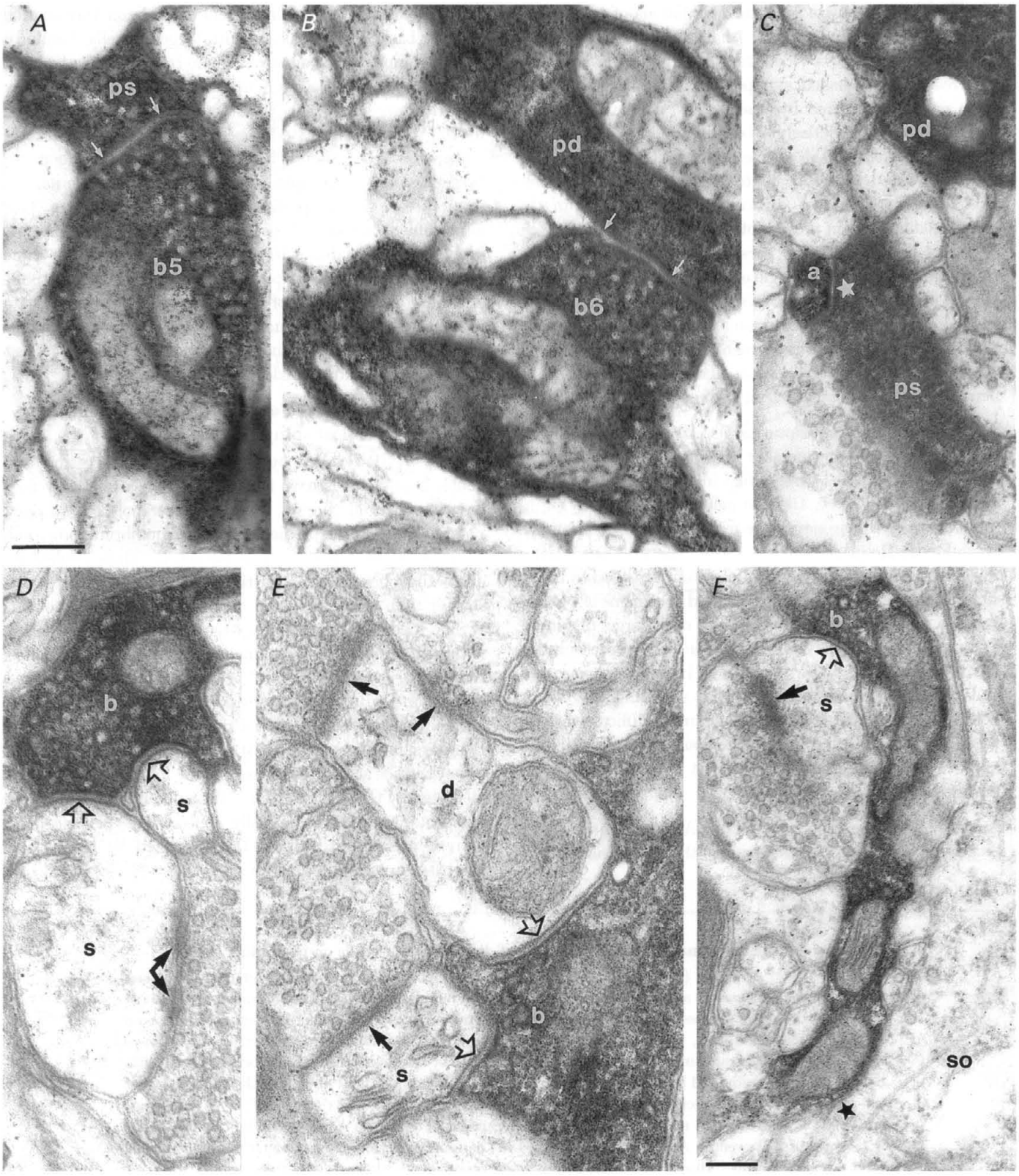

Figure 9. Electron microscopically identified synapses of double bouquet cells

A and *B*, identified synaptic junctions (between arrows) made by boutons (b5, b6) of the double bouquet cell and a spine (ps, in *A*) or a dendritic shaft (pd, in *B*) of the pyramidal cell shown in Fig. 8*A–E*. *C*, non-synaptic membrane apposition (star) between a thin axon (a) of the double bouquet and a spine (ps) of the pyramidal cell. *D* and *E*, boutons (b) of the double bouquet cell (DBC4) form synaptic junctions (open arrows) with dendritic spines (s) and a dendritic shaft (d) which also receive asymmetrical synapses (arrows)

IPSPs occurring in the perisomatic domain is largely shaped by passive membrane properties. Whether the slower decay of responses evoked by double bouquet cells was due to their distal dendritic location or the activation of different GABA receptors and/or voltage-gated conductances remains to be determined. Since single action potentials may not activate the full range of synaptic receptor mechanisms, the effects of short trains of action potentials was also tested, but the decay characteristics of the compound postsynaptic responses did not appear to be prolonged and, so far, no late $GABA_B$ receptor-mediated component has been revealed. However, Thomson *et al.* (1996) suggested the presence of a late component in the unitary IPSP following long duration firing of some presynaptic cells, although the location and number of the synapses mediating the effect were not reported.

The main target of neocortical excitatory synapses are dendritic spines (Kisvarday, Martin, Freund, Magloczky, Whitteridge & Somogyi, 1986), therefore terminals of double bouquet cells are strategically placed for the compartmental control of incoming excitatory input. Qian & Sejnowski (1990) proposed, on the basis of simulations, that inhibition on spines would be more effectively mediated by the activation of a K^+ conductance through $GABA_B$ receptors in comparison with the activation of a $GABA_A$ receptor mechanism. Our experimental evidence for the spine-targeting double bouquet cells, however, showed IPSP properties compatible with the activation of $GABA_A$ receptors. To our knowledge, this is the first recording of the activity and synaptic effect of double bouquet cells and the results strongly suggest that previous inferences for the GABAergic nature of this type of interneurone are likely to be correct (Somogyi & Cowey, 1981; DeFelipe & Jones, 1992). The GABAergic basket cells also form a significant proportion of their synapses on spines and evoke fast IPSPs. As we have not found a GABAergic unitary innervation directed exclusively to spines, we cannot exclude the possibility that the recorded postsynaptic effect was mediated solely by the release sites on dendritic shafts and the effect of synapses on spines was not detectable with conventional intrasomatic recording. This is unlikely, because excitatory synaptic responses evoked mostly on spines are readily recorded in the soma, and the slow rise and decay kinetics of $GABA_B$ receptor-mediated responses would be relatively unaffected by dendritic filtering. Furthermore, using glutamate-evoked activation of cortical cells, fast and slow inhibitory postsynaptic potentials were reported to be generated from separate sites (Benardo, 1994), or show differential activation depending on the site of microstimulation (Kang *et al.* 1994). The source of $GABA_B$ receptor-mediated synaptic responses remains to be established, and there are several additional GABAergic neuronal types innervating the dendritic domain (Somogyi, 1989) whose synaptic effect has not been tested.

Is there a pairing of GABAergic inputs with excitatory afferents on the dendritic domain?

The intracortical distribution of the axons of dendrite-targeting cells is similar to that of geniculo-cortical axons (Humphrey, Sur, Uhlrich & Sherman, 1985). Furthermore, the location of identified geniculo-cortical synaptic terminals on pyramidal cells in layers III–IV (Freund, Martin, Somogyi & Whitteridge, 1985; Friedlander & Martin, 1989) were in matching positions to those GABAergic synapses of dendrite-targeting cells demonstrated here in Fig. 4. Type I synapses targeting the same postsynaptic dendrite were frequently identified around the synapses established by dendrite-targeting cells. In the case of the GABAergic input to a spiny stellate cell, it is particularly striking that although any part of the somato-dendritic domain was within reach of the dendrite-targeting cell axon, only three proximal dendrites received synapses, equidistant from the soma, suggesting a constraint, possibly a co-stratification with geniculate input. These results lead us to propose the hypothesis that there is a subcellular pairing between the termination of thalamic afferents and terminals of dendrite-targeting cells, resulting in the grouped arrangement of dendrite-targeting cell terminals around thalamo-cortical synapses. Such a pairing has also been suggested in terms of space for some small basket cells (Kisvarday, Martin, Whitteridge & Somogyi, 1985; Somogyi, 1989; Kisvarday, 1992). This arrangement would allow appropriately timed fast IPSPs to rescale geniculate input-evoked EPSPs, preventing saturation and expanding the dynamic range of summation as suggested for the hippocampus (Halasy & Somogyi, 1993).

The dendrites of the type of pyramidal cell postsynaptic to the double bouquet cell are not present below the middle of layer III, therefore the columnar axon of the double bouquet cell, spanning all layers, innervates several populations of principal cells and may follow a particular glutamatergic input distributed similarly to a double bouquet axon. Of the possible glutamatergic axonal patterns in the visual cortex the most similar distribution of terminals is made by the axon collaterals of layer II–III pyramidal cells, which invariably make a patch of terminals in the vicinity of their cell bodies as well as in a patchy manner in layers II–III (Gilbert & Wiesel, 1983; Martin & Whitteridge, 1984) and descend in a narrow bundle through layer IV giving synapses mostly to dendritic spines (Kisvarday *et al.* 1986), as do double bouquet cells. Furthermore, double bouquet

from unlabelled terminals. *F*, the axon of a double bouquet cell (DBC2) fails to form a synapse (star) at a membrane apposition with an unlabelled soma (so), but its bouton (b) establishes a synaptic junction (open arrow) with an adjacent dendritic spine (s) which also receives an asymmetrical synapse (arrow) from another bouton. Scale bars, 0·2 μm; scale bar in *A* also applies to *B–E*.

cells are reciprocally innervated by the same superficial pyramidal cells that they innervate (Buhl *et al.* 1997). Thus, they may regulate the gain of local pyramidal cell interactions in the ensemble of a cortico-cortical axonal patch, terminating conjointly with pyramidal boutons on the same dendritic segments and spines.

The role of co-alignment of GABAergic and glutamatergic afferents on dendrites is not known, but several hypotheses have been suggested. In addition to the possible rescaling of EPSPs mentioned above, locally generated GABAergic effects may interact with other conductances. For example, dendritic GABAergic inputs may regulate the calcium components of dendritic action potentials (Miles, Tóth, Gulyás, Hajos & Freund, 1996), or e.g. dendrite-targeting cell terminals clustered close to dendritic branch points may attenuate the backpropagating action potentials during repetitive activation of pyramidal cells (Spruston, Schiller, Stuart & Sakmann, 1995). Since fast $GABA_A$ receptor-mediated IPSPs are likely to influence the activation of NMDA receptors and the duration of EPSPs, selective placement of GABAergic synapses on the dendrites provides a versatile mechanism to influence the window of EPSP temporal summation. The conjoint termination of specific GABAergic and glutamatergic afferents on the same segments of the dendrites may also lead to interactions between the two inputs through presynaptic $GABA_B$ receptors on the glutamatergic terminals, and/or presynaptic metabotropic glutamate receptors on the GABAergic terminals.

The number of synapses in unitary connections: IPSP amplitude and reliability

We demonstrated that neocortical interneurones innervate postsynaptic spiny cells via three to seventeen synaptic release sites. The overlap between the IPSP amplitude and recording noise distributions was inversely related to the number of synapses, indicating that a relatively high number of transmitter release sites restricts the number of postsynaptic response failures, as demonstrated by the absence of a distinct failure peak in the IPSP amplitude histograms. Thus, transmission at inhibitory connections remains reliable, even if the release probability was relatively low. Assuming binomial release statistics, an average of ten release sites and a uniform P value in the range of 0·3, the statistical likelihood for all terminals failing to release transmitter would be fairly small ($P < 10^{-5}$). Complete failures of synaptic transmission, however, may be attributable also to action potentials failing to invade both daughter branches of bifurcating axons. In this regard, our findings indicate the absence or extreme rarity of such branchpoint failures in the connections studied, because the respective terminals were located on axonal branches originating from 12th and 8th order axonal segments. It follows that any action potentials failing to invade lower order axonal branch points would have invariably resulted in a complete postsynaptic response failure. However, in view of the absence/rarity of such events any presynaptic factors affecting the response variability are thus likely to be restricted to either terminal branches and/or individual transmitter release sites.

The number of synapses in unitary connections: convergence and divergence

The number of synapses formed by the axons of the GABAergic cells revealed here are the highest reported for neocortical neurones, but the total number of synapses can only rarely be established from slice preparations. By selecting cells for analysis that were filled in the middle of the slice and judging from the decline of the density of axonal branches towards the cut surface of the slices, we estimated that at least 70–80% of the entire axonal arborization of even the most partial cell was within the reconstructed area. The contribution of a single GABAergic neurone to the total synapse population within the tissue volume occupied by the axon can be calculated using density data, and is unaffected by the loss of axonal processes (Table 2).

The tissue volume containing the axonal fields and the density of synapses formed by the individual interneurones was not significantly different between the three classes of cell. Taking the overall density of GABAergic synapses as 48×10^6 mm^{-3} (Beaulieu & Somogyi, 1990), the output of an average interneurone represents 0·66 ± 0·20% of the entire GABAergic synapse population. Due to their synaptic target selectivity, a significant difference emerges between the interneurone classes when the contribution of single interneurones to somatic, dendritic and spine GABAergic innervation is calculated (Table 2). Using the previous data on synaptic targets (Beaulieu & Somogyi, 1990) and taking into account the target distribution of cells reported here it emerges that a single basket cell provides about 2·1% of all somatic GABA-immunopositive synapses, whereas a dendrite-targeting cell provides only about 0·3% in a unit volume of tissue (Table 2). Similarly, an individual dendrite-targeting cell supplies about 1·1% of GABAergic synapses to dendritic shafts, which is higher than the fraction provided by a basket (~0·4%), or a double bouquet cell (~0·4%). An individual double bouquet cell provides about 1·9% of GABAergic synapses to dendritic spines within its axonal field, whereas the proportions of the other cells are markedly less.

If we assume that all neurones residing in the axonal field of an interneurone (1272 ± 414, using the density value of 50 000 mm^{-3}; Beaulieu & Colonnier, 1983) are innervated, each postsynaptic cell would be innervated by 4·31 ± 1·28 unitary GABAergic synapses. This number is lower than that obtained from the fully analysed cell pairs of this study (10·6 ± 5·6 synapses per postsynaptic cell). Therefore, either interneurones select some cells from the cell population within their axonal field, or possibly our physiological recordings were biased for detecting larger IPSPs mediated

by a relatively large number of release sites. A smaller number of synapses were reported in unitary connections in the rat (Thomson *et al.* 1996). The overall selectivity for postsynaptic cells could be much higher for interneurones having large, low density axonal fields such as the large basket cells (Somogyi *et al.* 1983; Kisvarday *et al.* 1993).

The number of presynaptic interneurones converging on the same postsynaptic cell can also be estimated on the somatic domain of pyramidal cells. The somata of callosal pyramidal cells in layer III were estimated to receive on average 252 synapses (Farinas & DeFelipe, 1991). Taking the number of synapses established by a single small basket cell on a pyramidal cell soma to be eleven, a convergence of about twenty-three basket cells on an individual pyramidal cell can be calculated. This estimate is very similar to the estimated twenty-five converging basket cells on a pyramidal cell in the hippocampus (Buhl *et al.* 1994). However, several types of basket cell, providing different densities of innervation, may converge onto each pyramidal cell in layer III, as large basket cells with wide-ranging axons were shown to provide only four to five synapses to individual pyramidal somata (Somogyi *et al.* 1983). Therefore, up to twenty-three to forty basket cells may converge on a layer III pyramidal neurone. At present, it is not possible to calculate the number of GABAergic cells converging on the dendritic region of pyramidal cells.

Parallels in the GABAergic innervation of neocortical and hippocampal principal cells

Several features of the GABAergic circuits revealed here are homologous to synaptic organization already found in the hippocampus (Halasy & Somogyi, 1993; Gulyás *et al.* 1993; Buhl *et al.* 1994). The main similarities are: (i) the segregation of somatic and multiple dendritic GABAergic innervation; (ii) the reflection of the overall target preference in the sites of termination on individual postsynaptic cells; (iii) the dual glutamatergic and GABAergic innervation of dendritic spines; (iv) the $GABA_A$ receptor-mediated unitary interactions mediated by GABAergic interneurones studied so far; (v) the summation characteristics of postsynaptic responses elicited by trains of action potentials of basket cells; (vi) the recurrent innervation of basket cells by pyramidal axon collaterals (Buhl *et al.* 1997); and (vii) the possible co-stratification of glutamatergic and GABAergic terminals on the dendritic domain of neocortical cells that is very striking in the hippocampus (see above). In the hippocampus the cell bodies of the relatively homogeneous populations of principal cells are aligned in a single lamina, and as a result the same tissue spaces contain functionally equivalent parts of principal cells, which makes it easier to recognize general principles of organization. Although the same principles appear to apply to the neocortex, in addition to the primary tangential innervation in the laminar neighbourhood of the GABAergic interneurones, their radially running axons also mediate interlaminar communication integrating distinct principal cell populations arranged in the column. A further differentiation in the neocortex is the specialization of the double bouquet cell and some basket cells for the GABAergic innervation of dendritic spines, which in the dentate gyrus are innervated by GABAergic neurones mainly innervating dendritic shafts (Halasy & Somogyi, 1993). Nonetheless, the overwhelming similarities in structural organization suggest that similar functional roles can be expected for the homologous cell types. For example, it is likely that the role of basket cells in the synchronization of the sub- and suprathreshold activity of principal cells demonstrated in the hippocampus (Cobb, Buhl, Halasy, Paulsen & Somogyi, 1995) will also apply to the neocortex where synchronous oscillatory activity is a prominent phenomenon (for review see Singer & Gray, 1995). Cortical basket cells evolved several distinct intra- and interlaminar axonal patterns that provide a versatile framework for the binding of the activity of a few hundred to a few thousand pyramidal cells through perisomatic $GABA_A$ receptor activation.

Avoli, M. (1986). Inhibitory potentials in neurons of the deep layers of the *in vitro* neocortical slice. *Brain Research* **370**, 165–170.

Beaulieu, C. & Colonnier, M. (1983). The number of neurons in the different laminae of the binocular and monocular regions of area 17 in the cat. *Journal of Comparative Neurology* **217**, 337–344.

Beaulieu, C. & Somogyi, P. (1990). Targets and quantitative distribution of GABAergic synapses in the visual cortex of the cat. *European Journal of Neuroscience* **2**, 296–303.

Benardo, L. S. (1994). Separate activation of fast and slow inhibitory postsynaptic potentials in rat neocortex *in vitro*. *Journal of Physiology* **476**, 203–215.

Buhl, E. H., Halasy, K. & Somogyi, P. (1994). Diverse sources of hippocampal unitary inhibitory postsynaptic potentials and the number of synaptic release sites. *Nature* **368**, 823–828.

Buhl, E. H., Tamás, G., Szilágyi, T., Stricker, C., Paulsen, O. & Somogyi, P. (1997). Effect, number and location of synapses made by single pyramidal cells onto aspiny interneurones of cat visual cortex. *Journal of Physiology* **500**, 689–713.

Cobb, S. R., Buhl, E. H., Halasy, K., Paulsen, O. & Somogyi, P. (1995). Synchronization of neuronal activity in hippocampus by individual GABAergic interneurons. *Nature* **378**, 75–78.

Connors, B. W., Malenka, R. C. & Silva, L. R. (1988). Two inhibitory postsynaptic potentials, and $GABA_A$ and $GABA_B$ receptor-mediated responses in neocortex of rat and cat. *Journal of Physiology* **406**, 443–468.

DeFelipe, J., Hendry, S. H. C., Hashikawa, T., Molinari, M. & Jones, E. G. (1990). A microcolumnar structure of monkey cerebral cortex revealed by immunocytochemical studies of double bouquet cell axons. *Neuroscience* **37**, 655–673.

DeFelipe, J. & Jones, E. G. (1992). High-resolution light and electron microscopic immunocytochemistry of colocalized GABA and calbindin D-28k in somata and double bouquet cell axons of monkey somatosensory cortex. *European Journal of Neuroscience* **4**, 46–60.

Deisz, R. A. & Prince, D. A. (1989). Frequency-dependent depression of inhibition in guinea-pig neocortex *in vitro* by $GABA_B$ receptor feed-back on GABA release. *Journal of Physiology* **412**, 513–541.

DEUCHARS, J. & THOMSON, A. M. (1995). Single axon fast inhibitory postsynaptic potentials elicited by a sparsely spiny interneuron in rat neocortex. *Neuroscience* **65**, 935–942.

FARINAS, I. & DEFELIPE, J. (1991). Patterns of synaptic input on corticocortical and corticothalamic cells in the cat visual cortex. I. The cell body. *Journal of Comparative Neurology* **304**, 53–69.

FREUND, T. F., MARTIN, K. A. C., SOMOGYI, P. & WHITTERIDGE, D. (1985). Innervation of cat visual areas 17 and 18 by physiologically identified X- and Y-type thalamic afferents. II. Identification of postsynaptic targets by GABA immunocytochemistry and Golgi impregnation. *Journal of Comparative Neurology* **242**, 275–291.

FRIEDLANDER, M. J. & MARTIN, K. A. C. (1989). Development of Y-axon innervation of cortical area 18 in the cat. *Journal of Physiology* **416**, 183–213.

GILBERT, C. D. & WIESEL, T. N. (1979). Morphology and intracortical projections of functionally characterised neurones in the cat visual cortex. *Nature* **280**, 120–125.

GILBERT, C. D. & WIESEL, T. N. (1983). Clustered intrinsic connections in cat visual cortex. *Journal of Neuroscience* **3**, 1116–1133.

GULYÁS, A. I., MILES, R., SÍK, A., TÓTH, K., TAMAMAKI, N. & FREUND, T. F. (1993). Hippocampal pyramidal cells excite inhibitory neurons through a single release site. *Nature* **366**, 683–687.

HALASY, K. & SOMOGYI, P. (1993). Subdivisions in the multiple GABAergic innervation of granule cells in the dentate gyrus of the rat hippocampus. *European Journal of Neuroscience* **5**, 411–429.

HUMPHREY, A. L., SUR, M., UHLRICH, D. J. & SHERMAN, S. M. (1985). Projection patterns of individual x- and y-cell axons from the lateral geniculate nucleus to cortical area 17 in the cat. *Journal of Comparative Neurology* **233**, 159–189.

KANG, Y., KANEKO, T., OHISHI, H., ENDO, K. & ARAKI, T. (1994). Spatiotemporally differential inhibition of pyramidal cells in the cat motor cortex. *Journal of Neurophysiology* **71**, 280–293.

KAWAGUCHI, Y. (1995). Physiological subgroups of nonpyramidal cells with specific morphological characteristics in layer II/III of rat frontal cortex. *Journal of Neuroscience* **15**, 2638–2655.

KISVARDAY, Z. F. (1992). GABAergic networks of basket cells in the visual cortex. *Progress in Brain Research* **90**, 385–405.

KISVARDAY, Z. F., BEAULIEU, C. & EYSEL, U. T. (1993). Network of GABAergic large basket cells in cat visual cortex (Area 18): implication for lateral disinhibition. *Journal of Comparative Neurology* **327**, 398–415.

KISVARDAY, Z. F., MARTIN, K. A. C., FREUND, T. F., MAGLOCZKY, Z., WHITTERIDGE, D. & SOMOGYI, P. (1986). Synaptic targets of HRP-filled layer III pyramidal cells in the cat striate cortex. *Experimental Brain Research* **64**, 541–552.

KISVARDAY, Z. F., MARTIN, K. A. C., WHITTERIDGE, D. & SOMOGYI, P. (1985). Synaptic connections of intracellularly filled clutch cells: a type of small basket cell in the visual cortex of the cat. *Journal of Comparative Neurology* **241**, 111–137.

MARTIN, K. A. C. & WHITTERIDGE, D. (1984). Form, function, and intracortical projections of spiny neurones in the striate visual cortex of the cat. *Journal of Physiology* **353**, 463–504.

MILES, R., TÓTH, K., GULYÁS, A. I., HAJOS, N. & FREUND, T. F. (1996). Differences between somatic and dendritic inhibition in the hippocampus. *Neuron* **16**, 815–823.

NEWBERRY, N. R. & NICOLL, R. A. (1985). Comparison of the action of baclofen with γ-aminobutyric acid on rat hippocampal pyramidal cells *in vitro*. *Journal of Physiology* **360**, 161–185.

QIAN, N. & SEJNOWSKI, T. J. (1990). When is an inhibitory synapse effective? *Proceedings of the National Academy of Sciences of the USA* **87**, 8145–8149.

SILLITO, A. M. (1992). GABA mediated inhibitory processes in the function of the geniculo-striate system. *Progress in Brain Research* **90**, 349–384.

SINGER, W. & GRAY, C. M. (1995). Visual feature integration and the temporal correlation hypothesis. *Annual Review of Neuroscience* **18**, 555–586.

SNEATH, P. H. A. & SOKAL, R. R. (1973). *Numerical Taxonomy*. W. H. Freeman & Co., San Francisco, CA, USA.

SOMOGYI, P. (1989). Synaptic organisation of GABAergic neurons and $GABA_A$ receptors in the lateral geniculate nucleus and visual cortex. In *Neural Mechanisms of Visual Perception. Proceedings of the Retina Research Foundation Symposia*, ed. LAM, D. K.-T. & GILBERT, C. D., pp. 35–62. Portfolio Publications, The Woodlands, TX, USA.

SOMOGYI, P. & COWEY, A. (1981). Combined Golgi and electron microscopic study on the synapses formed by double bouquet cells in the visual cortex of the cat and monkey. *Journal of Comparative Neurology* **195**, 547–566.

SOMOGYI, P., KISVARDAY, Z. F., MARTIN, K. A. C. & WHITTERIDGE, D. (1983). Synaptic connections of morphologically identified and physiologically characterized large basket cells in the striate cortex of cat. *Neuroscience* **10**, 261–294.

SPRUSTON, N., SCHILLER, Y., STUART, G. & SAKMANN, B. (1995). Activity-dependent action potential invasion and calcium influx into hippocampal CA1 dendrites. *Science* **268**, 297–300.

TAMÁS, G., BUHL, E. H. & SOMOGYI, P. (1995). Synaptic responses and effect of physiologically and anatomically identified double bouquet cells in cat visual cortex. *European Journal of Neuroscience*, suppl. 8, 76.

THOMSON, A. M., WEST, D. C., HAHN, J. & DEUCHARS, J. (1996). Single axon IPSPs elicited in pyramidal cells by three classes of interneurones in slices of rat neocortex. *Journal of Physiology* **496**, 81–102.

WARD, J. H. (1963). Hierarchical grouping to optimize an objective function. *Journal of the American Statistical Association* **58**, 236.

Acknowledgements

We are grateful to Dr Ole Paulsen and Dr Stuart Cobb for their comments on an earlier version of the manuscript, to Mr J. D. B. Roberts for technical assistance and to Mr P. Jays and Mr F. Kennedy for photographic assistance. G.T. held a Blaschko Visiting Research Scholarship and an Oxford–Szeged Scholarship during part of this project.

Author's email address

G. Tamás: gabor.tamas@pharm.ox.ac.uk

Received 29 July 1996; accepted 24 January 1997.